Energy Efficient Resource Allocation for Uplink RIS-Aided Millimeter-Wave Networks with NOMA

Xiangbin Yu, *Senior Member, IEEE*, Guangying Wang, Xu Huang, Kezhi Wang, *Senior Member, IEEE*, Weiye Xu, and Yun Rui, *Senior Member, IEEE*

Abstract—In this paper, energy efficiency (EE) is maximized for the reconfigurable intelligent surface (RIS) aided millimeter-Wave (mmWave) networks with non-orthogonal multiple access (NOMA) and multiple mobile devices. To this end, we first propose the EE optimization, under the constraints of maximum power, minimal rate of devices and constant modulus of beamforming (BF) vectors. Then, the joint resource allocation scheme of power allocation (PA) and BF is designed. Specifically, given PA, an effective iterative algorithm based on the majorization-minimization, concave-convex procedure and block coordinate descent (BCD) is presented to obtain closed-form solutions of suboptimal passive BF (PBF) and analog BF (ABF) for each iteration. Then, given PBF and ABF, an effective iterative algorithm based on the successive convex approximation, BCD and Dinkelbach methods is derived to achieve suboptimal closed-form PA for each iteration. By incorporating these two algorithms into the BCD method, a joint optimization algorithm for EE maximization is presented. As a result, joint resource allocation of PA, PBF and ABF is attained. Besides, the convergence and complexity of the algorithms are analyzed. For comparison, the benchmark scheme based on the multidimensional search method and artificial bee colony algorithm is also presented. Simulation results show that the proposed joint scheme is effective and higher EE can be obtained with lower complexity.

Index Terms—Energy efficiency, millimeter-wave communication, reconfigurable intelligent surface, power allocation, passive beamforming, analog beamforming.

I. INTRODUCTION

THE fifth generation (5G) and beyond wireless networks aim to achieve increasing network capacity and universal wireless connection. Millimeter wave (mmWave) communication could be applied to help alleviate the shortage of spectrum resources in the future communication networks, due to its wide spectrum [1], [2]. However, the mmWave channel is vulnerable to the blockage and subject to high propagation loss. Nevertheless, the limited transmission distance of mmWave communication makes it difficult to be applied in large-scale coverage. This problem can be effectively addressed by deploying the reconfigurable intelligent surface (RIS) in the system. The RIS can employ large number of low-cost passive reflection elements to improve the system performance in wireless propagation environment, and increase the coverage and connectivity of base stations (BS). Hence, it has been regarded as a promising technology for the next generation wireless communication networks [3]–[6]. Besides, non-orthogonal multiple access (NOMA) has been considered as a promising multiple access technique to support massive connectivity for 5G and beyond, which may also be applied in mmWave communication system to support more users and further improve the performance [7]–[9]. Based on the above discussions, the mmWave communication and RIS as well as NOMA can be effectively combined to improve the overall network performance, because of their high flexibility and huge bandwidth availability.

Besides, due to the significant increase of mobile devices and high data rate demand, the energy consumption is rapidly increased, which accounts for about five percent of the world energy consumption. Correspondingly, the energy consumption problem has become a challenging one in future wireless networks design. Based on this, pursuing high energy efficiency (EE) has received more and more concerns because of the environmental considerations. Hence, as a key performance index in 5G and beyond communication, the EE has attracted much more research interest in mmWave communication and RIS-aided communication [10]–[19]. The authors in [10] studied the mmWave system and proposed an optimal power control strategy based on the bisection method to maximize the EE of the system, and performance gain in both spectral efficiency (SE) and EE can be attained. A heuristic hybrid beamforming (BF) scheme was designed in [11] to improve the EE performance of a large-array mmWave system, where the simplified EE in consideration of the insertion loss was optimized. Using the NOMA technology, the authors in [12] studied the joint PA and BF designs for mmWave-NOMA system, and two suboptimal joint design schemes based on the one-dimensional search method were developed to increase the system EE. Simulation results verified the effectiveness of the proposed schemes. In [13], the authors investigated the EE performance of mmWave-NOMA with hybrid precoding, and the BF design was based on the given codebooks. For RIS communication, the resource allocation schemes were developed for downlink RIS-assisted multi-input single-output (MISO) in [14] to improve the EE performance, where the successive convex approximation (SCA) and greedy searching methods were respectively used for single user and multiuser case in the schemes. In [15], the authors proposed two resource allocation schemes based on the alternating maximization

X.Yu, G. Wang, X.Huang are with College of Electronic and Information Engineering, Nanjing University of Aeronautics and Astronautics, Nanjing, China. e-mail:(yxb-xwy@hotmail.com). K.Wang is with Department of Computer Science, Brunel University London, Uxbridge, Middlesex, UB8 3PH, United Kingdom. W. Xu is with School of Information and Communication Engineering, Nanjing Institute of Technology. Y. Rui is with the East China Normal University, Shanghai, China. X.Yu is also with State Key Laboratory of Millimeter Waves of Southeast University, China.

EE optimization in a RIS-based downlink multiuser MISO system, where the gradient descent and the sequential fractional programming were used for RIS designs, respectively, and the effectiveness of proposed schemes was verified by simulations. In [16], a joint design of transmit BF at access points and reflecting coefficients at RISs was presented to maximize the EE of RIS assisted cell-free network, which showed the benefit of using RISs, and a simple and efficient alternating algorithm was proposed to obtain the solution. By maximizing the system sum-rate of multiuser MISO downlink communications assisted by a self-sustainable intelligent reflection surface, the joint design of beamformers and the energy harvesting schedule was presented in [17], and an efficient iterative algorithm was proposed to obtain a suboptimal solution. In [18], the joint precoding at BSs and RIS for downlink RIS-aided cell-free network was designed by maximizing the weighted sum rate (WSR) to optimize the network capacity, and an alternating optimization scheme was proposed to solve the optimization problem and obtain the corresponding precoding design. With the proposed scheme, the network capacity can be increased greatly. In [19], the RIS was used to improve the cell-edge performance of downlink multicell multiple-input multiple-output (MIMO) systems, and joint design of the active transmit precoding of all base stations and the phase shifts at the RIS was presented to maximize the WSR of all users. By means of the weighted minimum mean-square error method and block coordinate descent (BCD) algorithm, an efficient iterative algorithm was proposed to obtain superior cell-edge performance over the conventional multicell system without RIS. However, these schemes above did not consider the integration of RIS and mmWave communications, and thus the performance improvement is limited. For this reason, [20]–[24] integrated the RIS in the mmWave communications to increase the overall performance. By maximizing the received signal power of RIS aided mmWave (RIS-mmWave) system, the authors in [20] derived an optimal closed-form solution for the single RIS case and obtained a near-optimal analytical solution for the multi-RIS case. In [21], by minimizing the mean-squared error between the received and the transmitted symbols, the BF design was presented for RIS-mmWave system, and the gradient-projection method was used to obtain the solution of BF. In [22], the total power of RIS-mmWave system was minimized by jointly optimizing the transmit powers of the devices, the multiuser detector at the base station (BS) and the passive BF at the RIS, and an alternating optimization algorithm was provided to solve the problem. In [23], by minimizing the transmit power at the BS under the signal-to-interference-plus-noise-ratio (SINR) constraints, the jointly design of hybrid BF at the BS and the response matrix at the RIS is presented for the RIS-aided downlink mmWave MIMO, and with this optimization design, the efficient power reduction can be attained. Besides, a sum rate optimization problem with respect to (w.r.t) the PA, active BF and passive BF was formulated for downlink RIS-assisted mmWave-NOMA system in [24], and an iterative algorithm based on the alternative optimization and SCA was proposed to solve the problem. With this algorithm, the system performance was effectively improved.

Based on the above analysis, the resource allocation schemes for sum-rate maximization and power minimization in RIS-mmWave communication were studied. However, there are few works to address the resource allocation schemes for energy efficient design in RIS-mmWave networks because of the challenging optimization, although some resource allocation schemes were developed for EE optimization in mmWave or RIS communication networks. Specifically, to our best knowledge, an energy-efficient joint resource allocation of PA, passive BF (PBF) and analog BF (ABF) for uplink RIS-mmWave with NOMA is not yet available in the literature. Motivated by the reasons above, the EE optimization of multi-device RIS aided mmWave-NOMA for jointly designing the PA and PBF as well as ABF over mmWave channel including light-of-sight (LOS) and non-light-of-sight (NLOS) paths is studied. Under the constraints of maximum power and constant-modulus (CM) as well as minimal rate, the constrained EE optimization problems are formulated. A joint design scheme is developed for achieving the corresponding resource allocations, and an efficient iterative algorithm is proposed to solve the optimization problem. With this scheme, superior EE performance is attained. The main contributions of this paper are summarized as follows:

1) The uplink RIS-assisted mmWave-NOMA network is presented and the RIS is used to aid the communication from the mobile devices to the BS to improve the network performance. The achievable sum rate and EE are firstly derived for performance evaluation and optimization. Then, with these results, a joint optimization problem for EE maximization is formulated subject to the constraints of the maximum transmit power, minimum rate of each device, the CM of the ABF and discrete CM of ABF vectors. For this problem, the PA of each device, the ABF of the BS and the PBF at the RIS are jointly optimized to maximize the EE.

2) Considering that the optimization problem of EE has the block structure, the BCD method is employed to tackle this problem. With this method, the original problem is firstly transformed into the subproblem of BF vectors design for the fixed PA and the subproblem of PA for the fixed BF vectors. For the fixed PA, an auxiliary variable is introduced and the penalty function method is utilized to deal with the BF design. Then, the BF design problem is decomposed into the design of PBF and ABF by means of the BCD method. With the bisection method and majorization-minimization (MM) method as well as the concave-convex procedure (CCCP) method, an effective iterative algorithm is proposed to tackle the joint BF design problem. As a result, suboptimal PBF and ABF with closed form are attained for each iteration.

3) For the fixed BF vectors, the SCA is utilized to transform the non-convex problem of PA into the convex problem. Then, using SCA, Dinkelbach and BCD methods, an effective iterative algorithm is proposed for solving PA optimization problem, where the solution of PA is derived in closed-form for each iteration. With two algorithms above, a joint optimization algorithm based on BCD method is proposed to obtain the suboptimal PA, PBF and ABF. Correspondingly, the energy-efficient resource allocation scheme is developed. After that, the complexity and convergence of the proposed algorithms

are analyzed. For comparison, the benchmark scheme (i.e., the second joint resource allocation scheme) is also presented based on the multidimensional search method and artificial bee colony (ABC) algorithm, which can obtain superior performance but with higher complexity.

4) Simulation results show that the proposed optimization scheme for the RIS-mmWave-NOMA is effective. With this scheme, the EE can be greatly increased and is much higher than that of the random phase based PBF scheme and the codebook based ABF scheme. Moreover, compared with the system without RIS, the proposed system can significantly improve the EE performance in mmWave communication. Moreover, the proposed scheme can achieve the EE performance near to that of the benchmark scheme but with lower complexity.

Notations: Vectors and matrices are respectively represented by boldface lower and upper case symbols. $(\cdot)^*$, $(\cdot)^T$ and $(\cdot)^H$ stand for the complex conjugate, the transpose and conjugate transpose, respectively. $|\cdot|$ and $\|\cdot\|$ represent the absolute value and 2-norm, respectively. $\text{Re}\{\cdot\}$ means taking the real part. $\mathcal{O}(\cdot)$ stands for the big-O notation. $\mathcal{CN}(\mathbf{0}, \mathbf{R})$ denotes the complex Gaussian distribution with zero-mean and covariance matrix $\mathbf{R}$, and $\text{U}[a, b]$ represents the uniform distribution in the interval $[a, b]$.

II. SYSTEM MODEL AND PROBLEM FORMULATION

A. System model

We consider an uplink RIS-mmWave network with NOMA and multiple mobile devices, as shown in Fig.1, where there are a BS with N antennas, K devices with a single antenna, a RIS with M reflection elements and one controller. The BS adopts the ABF architecture and requires one radio frequency chain (RFC). Each antenna connects to the RFC by a phase shifter (PS) and a lower noise amplifier (LNA), where N PSs and N LNAs are needed. In order to reduce the complexity of hardware implementation, all LNAs have the same amplification factor, such that the ABF vector $\mathbf{w} \in \mathbb{C}^{N \times 1}$ needs to meet the CM constraint [7], [8], [12], [25], i.e., $|[\mathbf{w}]_n| = 1/\sqrt{N}, \forall n \in 1, .., N$.

The BS receives the signals from devices in terms of uplink NOMA protocol, and a RIS assists the communication from the devices to the BS to improve the performance. The RIS reflection coefficients are calculated by the BS and fed back to the RIS controller through a dedicated link. It is supposed that the perfect channel state information (CSI) is available, which is also assumed in [14]- [24], and may be practically achieved by using different channel estimation methods [26]–[30]. At the transmitter, the signal transmitted by the k-th device (which is denoted as $\mathcal{U}_k$) is

$$s_k = \sqrt{p_k} x_k, \forall k \in \mathcal{K}, \tag{1}$$

where p_k and x_k are the transmit power and signal of $\mathcal{U}_k$, respectively, and the set $\mathcal{K}$ is defined as $\mathcal{K} \triangleq \{1, ..., K\}$.

Based on the uplink NOMA protocol [7]–[9] [12], the received signal at the BS after the ABF processing is given

by

$$
\begin{aligned}
y &= \sum_{k=1}^{K} \mathbf{w}^H(\mathbf{g}_k + \mathbf{H}\boldsymbol{\Theta}\mathbf{h}_k)s_k + \mathbf{w}^H\mathbf{n} \\
&= \sum_{k=1}^{K} \mathbf{w}^H(\mathbf{g}_k + \tilde{\mathbf{H}}_k\boldsymbol{\theta})s_k + \mathbf{w}^H\mathbf{n}, \forall k \in \mathcal{K},
\end{aligned}
\tag{2}
$$

where $\mathbf{n} \in \mathbb{C}^{N \times 1} \sim \mathcal{CN}(0, \sigma^2\mathbf{I}_N)$ is the noise vector, and its element has zero mean and variance σ^2, $\boldsymbol{\Theta} \in \mathbb{C}^{M \times M} = \text{diag}(\boldsymbol{\theta})$ is the PBF matrix of the RIS, in which the PBF vector $\boldsymbol{\theta} = [e^{j\theta_1}, ..., e^{j\theta_M}]^T$, θ_m is the phase shift of reflection coefficients, $\forall m \in \mathcal{M}$, where the set $\mathcal{M} \triangleq \{1, .., M\}$, and the amplitude of reflection coefficients is set as one to maximize the signal reflection. $\tilde{\mathbf{H}}_k = \mathbf{H}\text{diag}(\mathbf{h}_k)$ is the cascade channel. Besides, considering the hardware cost, the phase shifts $\{\theta_m\}$ can only be selected from a finite set of discrete values, which can be attained by uniformly quantizing the set of interval $[0, 2\pi)$. Specifically, the set of discrete phase shift values at each reflection element is given by [31], [24]

$$\Omega = \{0, \Delta\theta, ..., (L-1)\Delta\theta\} \tag{3}$$

where $\Delta\theta = 2\pi/L$, and L is the total number of discrete phase shift levels. Ideally, when L tends to be infinity, each element will have any phase-shift value in $[0, 2\pi)$, which corresponds to the continuous phase-shift case.

The mmWave channel vector $\mathbf{g}_k$ between $\mathcal{U}_k$ and the BS, $\mathbf{h}_k$ between $\mathcal{U}_k$ and the RIS, $\mathbf{H}$ between the RIS and the BS all adopt the Saleh-Valenzuela (SV) model. Specifically, the direct link $\mathbf{g}_k \in \mathbb{C}^{N \times 1}$ is modeled as

$$\mathbf{g}_k = \lambda_\text{U}\lambda_\text{B}\sqrt{\frac{N}{L_{k,\text{B}}}} \sum_{l=1}^{L_{k,\text{B}}} \alpha_{k,l}\mathbf{a}_\text{B}(N, \phi_{k,l}^{(\text{AoA})}), \tag{4}$$

where $\lambda_\text{U}, \lambda_\text{B}$ are the transmit gain and the receive gain, respectively. $L_{k,\text{B}}$ is the number of mmWave channel paths between $\mathcal{U}_k$ and the BS. $\alpha_{k,l}$ and $\phi_{k,l}^{(\text{AoA})}$ denote the complex gain coefficient and the angle of arrival for the l-th path of $\mathcal{U}_k$, respectively. $\mathbf{a}_\text{B}(N, \phi_{k,l}^{(\text{AoA})})$ is the array steering vector between $\mathcal{U}_k$ and the BS. It is defined that $\mathbf{a}(N, \Delta) = \frac{1}{\sqrt{N}}[1, e^{j\pi \sin \Delta}, ..., e^{j\pi(N-1)\sin \Delta}]^T$, where $\Delta \sim \text{U}[0, 2\pi]$.

The mmWave channel between $\mathcal{U}_k$ and the RIS, $\mathbf{h}_k \in \mathbb{C}^{M \times 1}$ is modeled as

$$\mathbf{h}_k = \lambda_\text{U}\lambda_\text{I}\sqrt{\frac{M}{L_{k,\text{I}}}} \sum_{l=0}^{L_{k,\text{I}}-1} \beta_{k,l}\mathbf{a}_\text{I}(M, \psi_{k,l}^{(\text{AoA})}), \tag{5}$$

where λ_I is the receive gain. $L_{k,\text{I}}$ is the number of mmWave channel paths between $\mathcal{U}_k$ and the RIS. $\beta_{k,l}$ and $\psi_{k,l}^{(\text{AoA})}$ denote the complex gain coefficient and the angle of arrival for the l-th path of $\mathcal{U}_k$, respectively. $\mathbf{a}_\text{I}(M, \psi_{k,l}^{(\text{AoA})})$ is the array steering vector between $\mathcal{U}_k$ and the RIS.

The mmWave channel between the RIS and the BS, $\mathbf{H} \in \mathbb{C}^{N \times M}$ is expressed as

$$\mathbf{H} = \lambda_\text{I}\lambda_\text{B}\sqrt{\frac{MN}{L_{\text{I,B}}}} \sum_{l=0}^{L_{\text{I,B}}-1} \beta_l\mathbf{a}_\text{B}(N, \psi_l^{(\text{AoA})})\mathbf{a}_\text{I}^H(M, \phi_l^{(\text{AoD})}),$$
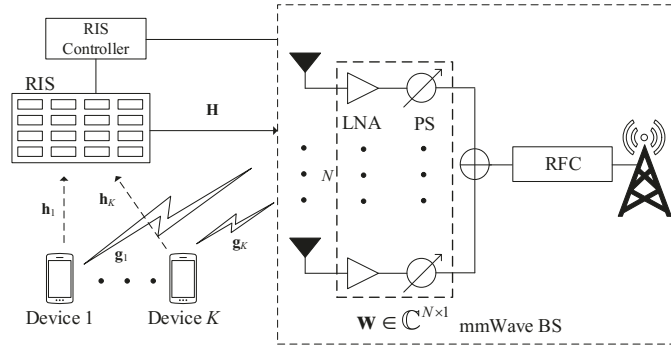
$$\tag{6}$$

Fig. 1.   Structure of uplink mmWave-RIS network with multiple devices.

where $L_{\mathrm{I,B}}$ is the number of mmWave channel paths between the RIS and the BS. β_l, $\psi_l^{(\mathrm{AoA})}$ and $\phi_l^{(\mathrm{AoD})}$ denote the complex gain coefficient, the angle of arrival and the angle of department for the l-th path, respectively. $\mathbf{a}_\mathrm{I}(M, \psi_l^{(\mathrm{AoA})})$ and $\mathbf{a}_\mathrm{B}(N, \psi_l^{(\mathrm{AoD})})$ are the array steering vectors between the RIS and the BS. Moreover, in (4), (5) and (6), $l = 0$ denotes the LOS path, while $l > 0$ denotes the NLOS path.

In order to process the superposed signal in (2), the BS employs the successive interference cancelation (SIC) scheme to decode the signal of users. For uplink NOMA, the SIC decoding order is the descending order of the effective channel gains of the users [7]–[9] generally, thus we need to consider the SIC decoding constraint $|\mathbf{w}^\mathrm{H}(\mathbf{g}_1 + \tilde{\mathbf{H}}_1\boldsymbol{\theta})|^2 \geq .... \geq |\mathbf{w}^\mathrm{H}(\mathbf{g}_K + \tilde{\mathbf{H}}_K\boldsymbol{\theta})|^2$ for optimization design, where $|\mathbf{w}^\mathrm{H}(\mathbf{g}_k + \tilde{\mathbf{H}}_k\boldsymbol{\theta})|^2$ is the effective channel gain of user k.

B. Problem formulation

Based on the analysis above, the EE optimization problem is formulated in this subsection. According to (2), using the SIC scheme and the decoding order, the SINR of $\mathcal{U}_k, \forall k \in \mathcal{K}$ can be derived as

$$\mathrm{SINR}_k = \frac{p_k \left|\mathbf{w}^\mathrm{H}(\mathbf{g}_k + \tilde{\mathbf{H}}_k\boldsymbol{\theta})\right|^2}{\sum_{j=k+1}^{K} p_j \left|\mathbf{w}^\mathrm{H}(\mathbf{g}_j + \tilde{\mathbf{H}}_j\boldsymbol{\theta})\right|^2 + \sigma^2}. \quad (7)$$

Thus, we can obtain the achievable rate of $\mathcal{U}_k$ as

$$\begin{aligned} R_k &= \log_2(1 + \mathrm{SINR}_k) \\ &= \log_2\left(1 + \frac{p_k|\mathbf{w}^\mathrm{H}(\mathbf{g}_k + \tilde{\mathbf{H}}_k\boldsymbol{\theta})|^2}{\sum_{j=k+1}^{K} p_j|\mathbf{w}^\mathrm{H}(\mathbf{g}_j + \tilde{\mathbf{H}}_j\boldsymbol{\theta})|^2 + \sigma^2}\right). \end{aligned} \quad (8)$$

According to the definition, the EE can be expressed as

$$\eta_{\mathrm{EE}} = \frac{\sum_{k=1}^{K} R_k}{\sum_{k=1}^{K} \nu p_k + P_\mathrm{C}} = \frac{\sum_{k=1}^{K} \log_2(1 + \mathrm{SINR}_k)}{\sum_{k=1}^{K} \nu p_k + P_\mathrm{C}} \quad (9)$$

where $\nu = \varrho^{-1}$, ϱ is the drain efficiency of the power amplifier, $P_\mathrm{C} = P_\mathrm{RF} + N P_\mathrm{PS} + N P_\mathrm{LNA} + P_\mathrm{BB} + P_\mathrm{RIS}$, in which $P_\mathrm{RF}, P_\mathrm{PS}, P_\mathrm{LNA}$, and P_BB are the power consumption of the RFC, PSs, LNAs and baseband, respectively [12], [13]. P_RIS is the power consumed by the RIS and it can be a constant [32], [33]. Therefore, under the maximum power, minimum

rate and CM constraints, the EE optimization problem can be formulated as

$$\begin{aligned} \mathrm{P0} : \max_{\{\mathbf{p},\mathbf{w},\boldsymbol{\theta}\}} \quad & \eta_{\mathrm{EE}} = \frac{\sum_{k=1}^{K} \log_2(1 + \mathrm{SINR}_k)}{\sum_{k=1}^{K} \nu p_k + P_\mathrm{C}} \\ \mathrm{s.t.} \quad & C_1 : |[\mathbf{w}]_n| = 1/\sqrt{N}, \forall n \in \mathcal{N}, \\ & C_2 : \theta_m \in \Omega, \forall m \in \mathcal{M}, \\ & C_3 : 0 \leq p_k \leq P_{\mathrm{max},k}, \forall k \in \mathcal{K}, \\ & C_4 : R_k \geq r_{0,k}, \\ & C_5 : |\mathbf{w}^\mathrm{H}(\mathbf{g}_1 + \tilde{\mathbf{H}}_1\boldsymbol{\theta})|^2 \geq .... \geq |\mathbf{w}^\mathrm{H}(\mathbf{g}_K + \tilde{\mathbf{H}}_K\boldsymbol{\theta})|^2, \end{aligned} \quad (10)$$

where the set $\mathcal{N} \triangleq \{1, ..., N\}$, $\mathbf{p} = [p_1, ..., p_K]^\mathrm{T}$, $P_{\mathrm{max},k}$ and $r_{0,k}$ are the maximum transmit power and minimum rate of $\mathcal{U}_k$, respectively.

By solving the optimization problem P0 above, we design a joint resource allocation scheme to maximize the EE. Since the P0 is non-convex fractional optimization problem and the number of the optimization variables is $M + N + K$, the complexity of directly searching the global optimal solution is extremely high considering that M and N are large in general. For this reason, a joint optimization algorithm based on the BCD method is proposed to solve the P0 taking the block structure of P0 into account. According to BCD method [34], [35], we alternatively optimize the PA $\mathbf{p}$ and BF vectors $\{\mathbf{w}, \boldsymbol{\theta}\}$ in problem P0. Thus, the P0 is divided into two subproblems P1 and P2. We firstly solve the problem P1 w.r.t $\{\mathbf{w}, \boldsymbol{\theta}\}$ given $\mathbf{p}$, and then solve the problem P2 w.r.t $\{\mathbf{p}\}$ given $\{\mathbf{w}, \boldsymbol{\theta}\}$ until they converge. Hence, in the following two sections, we will present a design of BF vectors $\{\mathbf{w}, \boldsymbol{\theta}\}$ given PA $\mathbf{p}$ and a design of $\mathbf{p}$ given $\{\mathbf{w}, \boldsymbol{\theta}\}$, which are performed at the t-th iteration of BCD method.

In order to deal with the problem (10), we first relax the discrete values of $\{\theta_m\}$ into continuous values, i.e., $\theta_m \in [0, 2\pi]$, and then map the attained continuous phase shifts to the nearest discrete values in $[0, 2\pi]$. Correspondingly, $|[\boldsymbol{\theta}]_m| = 1$. Thus, the optimization problem (10) is transformed into

$$\begin{aligned} \tilde{\mathrm{P}}0 : \max_{\{\mathbf{p},\mathbf{w},\boldsymbol{\theta}\}} \quad & \eta_{\mathrm{EE}} = \frac{\sum_{k=1}^{K} \log_2(1 + \mathrm{SINR}_k)}{\sum_{k=1}^{K} \nu p_k + P_\mathrm{C}} \\ \mathrm{s.t.} \quad & C_1, C_3, C_4, C_5, \\ & \tilde{C}_2 : |[\boldsymbol{\theta}]_m| = 1, \forall m \in \mathcal{M}. \end{aligned} \quad (11)$$

III. BEAMFORMING DESIGN

In this section, we will design the BF vectors for the joint optimization scheme, and provide the solution of $\{\mathbf{w}, \boldsymbol{\theta}\}$ for given $\mathbf{p}$ by solving problem P1.

With (11) and (7), given $\mathbf{p}$, the BF problem w.r.t $\{\mathbf{w}, \boldsymbol{\theta}\}$ is formulated as

$$\text{P1}: \max_{\{\mathbf{w}, \boldsymbol{\theta}\}} \quad \sum_{i=1}^{K} \log\left(1 + \frac{p_i|\mathbf{w}^{\text{H}}(\mathbf{g}_i + \tilde{\mathbf{H}}_i\boldsymbol{\theta})|^2}{\sum_{j=i+1}^{K} p_j|\mathbf{w}^{\text{H}}(\mathbf{g}_j + \tilde{\mathbf{H}}_j\boldsymbol{\theta})|^2 + \sigma^2}\right)$$
$$\text{s.t. } C_1, \tilde{C}_2, C_4, C_5, \tag{12}$$

where $\log(2)$ is omitted because it is a constant and does not affect the optimization result.

Since the problem P1 is difficult to be solved directly, we introduce the auxiliary variable $z_i = |\mathbf{w}^{\text{H}}(\mathbf{g}_i + \tilde{\mathbf{H}}_i\boldsymbol{\theta})|^2 (i \in \mathcal{K})$ for dealing with the P1, and the corresponding P1 is rewritten as

$$\bar{\text{P1}}: \max_{\{\mathbf{z}, \mathbf{w}, \boldsymbol{\theta}\}} \quad \sum_{i=1}^{K} \log\left(1 + \frac{p_k z_i}{\sum_{j=i+1}^{K} p_j z_j + \sigma^2}\right)$$
$$\text{s.t. } C_1, \tilde{C}_2, C_4, \tag{13}$$
$$C_6 : z_i = |\mathbf{w}^{\text{H}}(\mathbf{g}_i + \tilde{\mathbf{H}}_i\boldsymbol{\theta})|^2, \forall i \in \mathcal{K}$$
$$\tilde{C}_5 : z_1 \geq ... \geq z_K.$$

where $\mathbf{z} = [z_1, z_2, ..., z_K]^T$. By using the penalty function method [36], the equality constraint is moved into the objective function. Then $\bar{\text{P1}}$ is reformulated as

$$\tilde{\text{P1}}:$$
$$\max_{\{\mathbf{z}, \mathbf{w}, \boldsymbol{\theta}\}} \quad \sum_{i=1}^{K} \log\left(1 + \frac{p_i z_i}{\sum_{j=i+1}^{K} p_j z_j + \sigma^2}\right)$$
$$- \frac{1}{2}\rho^{(l)} \sum_{i=1}^{K} \left(\sqrt{z_i} - |\mathbf{w}^{\text{H}}(\mathbf{g}_i + \tilde{\mathbf{H}}_i\boldsymbol{\theta})|\right)^2 \tag{14}$$
$$\text{s.t. } C_1, \tilde{C}_2, C_4, \tilde{C}_5,$$

where $\rho^{(l-1)}$ is the penalty coefficient at the $(l-1)$-th iteration of penalty method which is updated according to $\rho^{(l)} = c\rho^{(l-1)}(c > 1)$.

In order to solve the problem $\tilde{\text{P1}}$, we decompose $\tilde{\text{P1}}$ into three subproblems based on BCD method by iteratively optimizing one optimization variable with the others being fixed. In particular, the following steps are carried out at the r-th iteration of BCD method.

A. Solving $\mathbf{z}$ given $\{\mathbf{w}, \boldsymbol{\theta}\}$

With (14), given $\{\mathbf{w}, \boldsymbol{\theta}\}$, the subproblem w.r.t $\mathbf{z}$ is formulated as

$$\text{P1.1}:$$
$$\max_{\mathbf{z}} \quad J_1 = \sum_{i=1}^{K} \log\left(1 + \frac{p_i z_i}{\sum_{j=i+1}^{K} p_j z_j + \sigma^2}\right) \tag{15}$$
$$- \frac{1}{2}\rho^{(l)} \sum_{i=1}^{K} \left(\sqrt{z_i} - |\mathbf{w}^{\text{H}}(\mathbf{g}_i + \tilde{\mathbf{H}}_i\boldsymbol{\theta})|\right)^2.$$

It is observed that the objective function J_1 in problem P1.1 has a special form, i.e., it is the difference of concave (D.C.)

functions [37]. According to this, the CCCP method [37] is employed to tackle this problem to obtain the optimized $\mathbf{z}$. With the CCCP method, the J_1 of the problem P1.1 becomes J_2 in (16), which is shown at the top of next page, where $z_i^{(n-1)}$ is the value of z_i at the $(n-1)$-th iteration of CCCP method.

By removing the constant term and letting $\xi_i = |\mathbf{w}^{\text{H}}(\mathbf{g}_i + \tilde{\mathbf{H}}_i\boldsymbol{\theta})|$, the problem P1.1 is transformed into

$$\bar{\text{P1.1}}: \max_{\mathbf{z}} J_3 =$$
$$\sum_{k=1}^{K} \log\left(\sum_{i=k}^{K} p_i z_i + \sigma^2\right) - \sum_{k=1}^{K}\sum_{i=1}^{k-1} \frac{z_k p_k}{\sum_{j=i+1}^{K} p_j z_j^{(n-1)} + \sigma^2}$$
$$- \frac{1}{2}\rho^{(l)} \sum_{i=1}^{K} \left(\sqrt{z_i} - \xi_i\right)^2. \tag{17}$$

It is shown that the problem $\bar{\text{P1.1}}$ is convex, so the optimal solution of z_k can be attained by solving the $\frac{\partial J_3}{\partial z_k} = 0$. With (17), we can calculate $\frac{\partial J_3}{\partial z_k}$ as

$$\frac{\partial J_3}{\partial z_k} = f(z_k)$$
$$= \sum_{i=1}^{k} \frac{p_k}{\sum_{j=i}^{K} p_j z_j + \sigma^2} - \sum_{i=1}^{k-1} \frac{p_k}{\sum_{j=i+1}^{K} p_j z_j^{(n-1)} + \sigma^2}$$
$$= \sum_{i=1}^{k} \frac{p_k}{p_k z_k + \tilde{I}_{1,ik}} - \tilde{I}_{2,k} - \frac{1}{2}\rho^{(l)}\left(1 - \frac{\xi_k}{\sqrt{z_k}}\right) \tag{18}$$

where $\tilde{I}_{1,ik} = \sum_{j=i, \neq k}^{K} p_j z_j + \sigma^2$ and $\tilde{I}_{2,k} = p_k \sum_{i=1}^{k-1} \frac{1}{\sum_{j=i+1}^{K} p_j z_j^{(n-1)} + \sigma^2}$.

In the following, we introduce the Lemma 1 to show that $f(z_k) = 0$ has a unique solution.

Lemma 1: The equation $f(z_k) = 0$ has a unique solution of z_k.

Proof: Please see Appendix A. ∎

Based on the Lemma 1, we can employ the simple bisection method to obtain the optimal solution of $f(z_k) = 0$, i.e., z_k^o. Correspondingly, $z_k^{(n)}$ is updated by z_k^o for $k = 1, ...K$. Based on this, using the CCCP method and iterative calculation, a near-optimal z_k^{nop} is attained. Considering the C_4 constraint, $z_k^{(r)}$ is updated by

$$z_k^{(r)} = \max\{z_k^{\text{nop}}, z_{k,\min}\}, \forall k \in \mathcal{K}, \tag{19}$$

where $z_{k,\min} = (2^{r_{0,k}} - 1)p_k^{-1}(\sum_{j=k+1}^{K} p_j z_j + \sigma^2)$. Furthermore, considering the $\tilde{C}_5$ constraint, we have:

$$z_k^{(r)} = \max\{z_k^{(r)}, z_{k+1}^{(r)}\}, \ k = 1, ..., K-1. \tag{20}$$

B. Solving $\boldsymbol{\theta}$ given $\{\mathbf{z}, \mathbf{w}\}$

Given $\{\mathbf{z}, \mathbf{w}\}$, the subproblem w.r.t $\boldsymbol{\theta}$ is formulated as

$$\text{P1.2}: \min_{\boldsymbol{\theta}} \quad \sum_{i=1}^{K} \left(\sqrt{z_i} - |\mathbf{w}^{\text{H}}(\mathbf{g}_i + \tilde{\mathbf{H}}_i\boldsymbol{\theta})|\right)^2 \tag{21}$$
$$\text{s.t. } |[\boldsymbol{\theta}]_m| = 1, \forall m \in \mathcal{M}.$$

$$J_2 = K \log \left(\sum_{j=1}^{K} p_j z_j + \sigma^2 \right) - \sum_{i=1}^{K} \log \left(\sum_{j=i+1}^{K} p_j z_j^{(n-1)} + \sigma^2 \right) - \sum_{k=1}^{K} \sum_{i=1}^{k-1} \frac{(z_k - z_k^{(n-1)}) p_k}{\sum_{j=i+1}^{K} p_j z_j^{(n-1)} + \sigma^2}$$
$$- \frac{1}{2} \rho^{(l)} \sum_{i=1}^{K} \left(\sqrt{z_i} - |\mathbf{w}^H (\mathbf{g}_i + \tilde{\mathbf{H}}_i \boldsymbol{\theta})| \right)^2, \tag{16}$$

Since $\mathbf{z}$ and $\mathbf{w}$ are known, the problem P1.2 is equivalent to

$$\tilde{P}1.2 : \min_{\boldsymbol{\theta}} \quad \sum_{i=1}^{K} |\mathbf{w}^H (\mathbf{g}_i + \tilde{\mathbf{H}}_i \boldsymbol{\theta})|^2 - 2\sqrt{z_i} |\mathbf{w}^H (\mathbf{g}_i + \tilde{\mathbf{H}}_i \boldsymbol{\theta})|$$
$$\text{s.t.} \ |[\boldsymbol{\theta}]_m| = 1, \forall m \in \mathcal{M}. \tag{22}$$

Considering the effectiveness of the MM method [38], we can use it to solve the problem $\tilde{P}1.2$. Let $\mathbf{f}_i = \mathbf{g}_i + \tilde{\mathbf{H}}_i \boldsymbol{\theta}$, then we have:

$$|\mathbf{w}^H \mathbf{f}_i| \geq \frac{\text{Re} \left\{ \mathbf{w}^H \mathbf{f}_i \left(\mathbf{f}_i^{(s-1)} \right)^H \mathbf{w} \right\}}{\left| \mathbf{w}^H \mathbf{f}_i^{(s-1)} \right|}, \tag{23}$$

where $\mathbf{f}_i^{(s-1)}$ is the $(s-1)$-th iteration of $\mathbf{f}_i$, and (23) can be obtained by the following Lemma 2.

Lemma 2: For two complex numbers $\tilde{x}$ and $\tilde{y}$, it can be shown that

$$|\tilde{x}||\tilde{y}| \geq \text{Re}\{\tilde{x}\tilde{y}^*\}. \tag{24}$$

Proof: Please see Appendix B. ∎

With (23), the convex majorization problem for (22) is given by

$$\bar{P}1.2 : \min_{\boldsymbol{\theta}} \quad \sum_{i=1}^{K} \left| t_i - \mathbf{w}^H \mathbf{f}_i \right|^2$$
$$\text{s.t.} \ |[\boldsymbol{\theta}]_m| = 1, \forall m \in \mathcal{M}, \tag{25}$$

where $t_i = \sqrt{z_i} \frac{\mathbf{w}^H \mathbf{f}_i^{(s-1)}}{|\mathbf{w}^H \mathbf{f}_i^{(s-1)}|}, \forall i \in \mathcal{K}$. Considering that

$$\left| t_i - \mathbf{w}^H \mathbf{f}_i \right|^2 = |t_i - \mathbf{w}^H \mathbf{g}_i - \mathbf{w}^H \tilde{\mathbf{H}}_i \boldsymbol{\theta}|^2$$
$$= \boldsymbol{\theta}^H \left(\tilde{\mathbf{H}}_i^H \mathbf{w} \mathbf{w}^H \tilde{\mathbf{H}}_i \right) \boldsymbol{\theta}$$
$$- 2\text{Re} \left(\boldsymbol{\theta}^H \left(\tilde{\mathbf{H}}_i^H \mathbf{w} \left(t_i - \mathbf{w}^H \mathbf{g}_i \right) \right) \right)$$
$$+ \left| t_i - \mathbf{w}^H \mathbf{g}_i \right|^2, \tag{26}$$

the problem $\bar{P}1.2$ is reformulated as

$$\check{P}1.2 : \min_{\boldsymbol{\theta}} \quad \boldsymbol{\theta}^H \mathbf{V} \boldsymbol{\theta} - 2\text{Re} \left\{ \boldsymbol{\theta}^H \tilde{\mathbf{v}} \right\} + \bar{v}$$
$$\text{s.t.} \ |[\boldsymbol{\theta}]_m| = 1, \forall m \in \mathcal{M}, \tag{27}$$

where $\mathbf{V} = \sum_{i=1}^{K} \tilde{\mathbf{H}}_i^H \mathbf{w} \mathbf{w}^H \tilde{\mathbf{H}}_i$, $\tilde{\mathbf{v}} = \sum_{i=1}^{K} \tilde{\mathbf{H}}_i^H \mathbf{w} \left(t_i - \mathbf{w}^H \mathbf{g}_i \right)$, and $\bar{v} = \sum_{i=1}^{K} |t_i - \mathbf{w}^H \mathbf{g}_i|^2$.

Given $\boldsymbol{\theta}^{(s-1)}$, the value of $\boldsymbol{\theta}$ at the $(s-1)$-th iteration of MM algorithm, the tight upper bound of $\boldsymbol{\theta}^H \mathbf{V} \boldsymbol{\theta}$ is given by [38]

$$\boldsymbol{\theta}^H \mathbf{V} \boldsymbol{\theta} \leq \boldsymbol{\theta}^H \hat{\mathbf{V}} \boldsymbol{\theta} - 2\text{Re} \left\{ \boldsymbol{\theta}^H \mathbf{e}^{(s-1)} \right\} + \left(\boldsymbol{\theta}^{(s-1)} \right)^H \mathbf{e}^{(s-1)}, \tag{28}$$

where $\mathbf{e}^{(s-1)} = \left(\hat{\mathbf{V}} - \mathbf{V} \right) \boldsymbol{\theta}^{(s-1)}$, $\hat{\mathbf{V}} = \lambda_{\max}(\mathbf{V}) \mathbf{I}_M$, $\lambda_{\max}(\mathbf{V})$ is the maximum eigenvalue of $\mathbf{V}$ which is from the eigenvalue decomposition (EVD) of $\mathbf{V}$. For the feasible solution $\boldsymbol{\theta}$ in (27), $\boldsymbol{\theta}^H \hat{\mathbf{V}} \boldsymbol{\theta} = M \lambda_{\max}(\mathbf{V})$ is a constant. Discarding the constants independent of $\boldsymbol{\theta}$, problem $\check{P}1.2$ is approximated as

$$\hat{P}1.2 : \max_{\boldsymbol{\theta}} \quad \text{Re} \left\{ \boldsymbol{\theta}^H \tilde{\mathbf{e}}^{(s-1)} \right\}$$
$$\text{s.t.} \ |[\boldsymbol{\theta}]_m| = 1, \forall m \in \mathcal{M}, \tag{29}$$

where $\tilde{\mathbf{e}}^{(s-1)} = \mathbf{e}^{(s-1)} + \tilde{\mathbf{v}}$.

The problem $\hat{P}1.2$ can be divided into M subproblems as follows:

$$\text{P1.2.1} : \max_{\vartheta_m} \quad \cos \left\{ \upsilon_m^{(s-1)} - \vartheta_m \right\}$$
$$\text{s.t.} \ 0 < \vartheta_m < 2\pi, \forall m \in \mathcal{M}, \tag{30}$$

where $\upsilon_m^{(s-1)}$ and ϑ_m are the phases of $[\tilde{\mathbf{e}}^{(s-1)}]_m$ and $[\boldsymbol{\theta}]_m$, respectively. Obviously, the optimal solution of the problem P1.2.1 is $\vartheta_m^{\text{opt}} = \upsilon_m^{(s-1)}, \forall m \in \mathcal{M}$. Thus, the solution of $\hat{P}1.2$ is given by

$$\boldsymbol{\theta}^o = \left[\exp(j\vartheta_1^{\text{opt}}), ..., \exp(j\vartheta_M^{\text{opt}}) \right]^T. \tag{31}$$

Correspondingly, $\boldsymbol{\theta}^{(s)}$ is updated by $\boldsymbol{\theta}^{(s)} = \boldsymbol{\theta}^o$. Based on this, using the MM algorithm and iterative calculation, suboptimal $\boldsymbol{\theta}$, $\boldsymbol{\theta}^{\text{sub}}$ is achieved. Thus, $\boldsymbol{\theta}^{(r)}$ is updated by

$$\boldsymbol{\theta}^{(r)} = \boldsymbol{\theta}^{\text{sub}}. \tag{32}$$

As a summary, the MM algorithm for solving P1.2 is shown as follows:

Algorithm 1 MM algorithm for solving the problem P1.2

1: **Initialize**: iteration index $s = 0$, iteration tolerance $\varepsilon > 0$, initial point $\boldsymbol{\theta}^{(0)}$;
2: **repeat**
3:    $s = s + 1$;
4:    Update $\boldsymbol{\theta}^{(s)}$ according to (31);
5: **until** $\|\boldsymbol{\theta}^{(s)} - \boldsymbol{\theta}^{(s-1)}\| < \varepsilon$
6: **Output**: $\boldsymbol{\theta}^{(s)}$.

Considering that the above obtained phase shift is continuous, we present the suboptimal passive BF with discrete phase shifts by using the phase quantization based on the continuous phase shifts. Namely, we map the obtained phase shifts to the nearest discrete values in $[0, 2\pi)$, which can be given by

$$\theta_m = \arg \min_{\theta \in \Omega} | \exp(j\theta) - [\boldsymbol{\theta}^{\text{sub}}]_m|, \forall m \in \mathcal{M}. \tag{33}$$

Note that the newly achieved solution of $\{\theta_m\}$ may not be optimal, to guarantee that the proposed algorithm converges,

the solution $\{\theta_m\}$ is updated only when the objective functions value in (13) increases [24].

C. Solving $\mathbf{w}$ given $\mathbf{z}$ and $\boldsymbol{\theta}$

Given $\mathbf{z}$ and $\boldsymbol{\theta}$, $\{\mathbf{f}_i = \mathbf{g}_i + \tilde{\mathbf{H}}_i\boldsymbol{\theta}\}$ are known, the subproblem w.r.t $\mathbf{w}$ can be formulated as

$$\text{P1.3}: \min_{\mathbf{w}} \quad \sum_{i=1}^{K}\left(\sqrt{z_i} - \left|\mathbf{w}^{\mathrm{H}}\mathbf{f}_i\right|\right)^2 = \sum_{i=1}^{K}\left(\sqrt{z_i} - \left|\mathbf{f}_i^{\mathrm{H}}\mathbf{w}\right|\right)^2$$
$$\text{s.t.} \quad [\mathbf{w}]_n = 1/\sqrt{N}, \forall n \in \mathcal{N}. \tag{34}$$

It can be found that the problem P1.3 is very similar to P1.2. Thus, MM algorithm can also be used for solving $\mathbf{w}$ in problem P1.3.

Based on Lemma 2, we have:

$$\left|\mathbf{f}_i^{\mathrm{H}}\mathbf{w}\right| \geq \frac{\mathrm{Re}\left\{\mathbf{f}_i^{\mathrm{H}}\mathbf{w}\left(\mathbf{w}^{(\iota-1)}\right)^{\mathrm{H}}\mathbf{f}_i\right\}}{\left|\mathbf{f}_i^{\mathrm{H}}\mathbf{w}^{(\iota-1)}\right|}, \tag{35}$$

where $\mathbf{w}^{(\iota-1)}$ is the value of $\mathbf{w}$ at the $(\iota-1)$-th iteration of MM algorithm, using the analytical method in (21)-(25), the problem P1.3 can be changed into

$$\bar{\text{P}}1.3: \quad \begin{array}{c} \min_{\mathbf{w}} \quad \sum_{i=1}^{K}\left|q_i - \mathbf{f}_i^{\mathrm{H}}\mathbf{w}\right|^2 \\ \text{s.t.} \quad |[\mathbf{w}]_n| = 1/\sqrt{N}, \forall n \in \mathcal{N}, \end{array} \tag{36}$$

where $q_i = \sqrt{z_i}\frac{\mathbf{f}_i^{\mathrm{H}}\mathbf{w}^{(\iota-1)}}{|\mathbf{f}_i^{\mathrm{H}}\mathbf{w}^{(\iota-1)}|}, \forall i \in \mathcal{K}$.

Therefore, the problem $\bar{\text{P}}1.3$ is equivalent to

$$\tilde{\text{P}}1.3: \quad \begin{array}{c} \min_{\mathbf{w}} \quad \mathbf{w}^{\mathrm{H}}\mathbf{S}\mathbf{w} - 2\,\mathrm{Re}\left\{\mathbf{w}^{\mathrm{H}}\tilde{\mathbf{s}}\right\} + \bar{s} \\ \text{s.t.} \quad |[\mathbf{w}]_n| = 1/\sqrt{N}, \forall n \in \mathcal{N}, \end{array} \tag{37}$$

where $\mathbf{S} = \sum_{i=1}^{K}\mathbf{f}_i\mathbf{f}_i^{\mathrm{H}}$, $\tilde{\mathbf{s}} = \sum_{i=1}^{K}\mathbf{f}_iq_i$, $\bar{s} = \sum_{i=1}^{K}|q_i|^2$.

Given $\mathbf{w}^{(\iota-1)}$, the tight upper bound of $\mathbf{w}^{\mathrm{H}}\mathbf{S}\mathbf{w}$ is

$$\mathbf{w}^{\mathrm{H}}\mathbf{S}\mathbf{w} \leq \mathbf{w}^{\mathrm{H}}\hat{\mathbf{S}}\mathbf{w} - 2\,\mathrm{Re}\left\{\mathbf{w}^{\mathrm{H}}\mathbf{b}^{(\iota-1)}\right\} + \left(\mathbf{w}^{(\iota-1)}\right)^{\mathrm{H}}\mathbf{b}^{(\iota-1)}, \tag{38}$$

where $\mathbf{b}^{(\iota-1)} = (\hat{\mathbf{S}} - \mathbf{S})\mathbf{w}^{(\iota-1)}$, $\hat{\mathbf{S}} = \lambda_{\max}(\mathbf{S})\mathbf{I}_N$.

Considering that $\mathbf{w}^{\mathrm{H}}\hat{\mathbf{S}}\mathbf{w} = \lambda_{\max}(\mathbf{S})$ is a constant, and removing the constants independent of $\mathbf{w}$, the problem $\tilde{\text{P}}1.3$ is approximated as

$$\hat{\text{P}}1.3: \max_{\mathbf{w}} \quad \mathrm{Re}\left\{\mathbf{w}^{\mathrm{H}}\tilde{\mathbf{b}}^{(\iota-1)}\right\}$$
$$\text{s.t.} \quad |[\mathbf{w}]_n| = 1/\sqrt{N}, \forall n \in \mathcal{N}, \tag{39}$$

where $\tilde{\mathbf{b}}^{(\iota-1)} = \mathbf{b}^{(\iota-1)} + \tilde{\mathbf{s}}$. The problem $\hat{\text{P}}1.3$ can be divided into N subproblems:

$$\text{P1.3.1}: \max_{\vartheta_n'} \quad \cos\left((v_n')^{(\iota-1)} - \vartheta_n'\right)$$
$$\text{s.t.} \quad 0 \leq \vartheta_n' \leq 2\pi, \tag{40}$$

where v_n' and ϑ_n' are the phases of $[\tilde{\mathbf{b}}^{(\iota-1)}]_n$ and $[\mathbf{w}]_n$, respectively. Obviously, the optimal solution of the problem P1.3.1 is $\vartheta_n'^{\text{opt}} = v_n'^{(\iota-1)}, \forall n \in \mathcal{N}$. Correspondingly, the solution of $\hat{\text{P}}1.3$ is given by

$$\mathbf{w}^o = \left[\exp(jv_1')^{(\iota-1)}, \ldots, \exp(jv_N')^{(\iota-1)}\right]^{\mathrm{T}}/\sqrt{N}. \tag{41}$$

Hence, $\mathbf{w}^{(\iota)}$ is updated by $\mathbf{w}^{(\iota)} = \mathbf{w}^o$. Based on this, using the MM algorithm and iterative calculation, suboptimal $\mathbf{w}$, $\mathbf{w}^{\text{sub}}$ is achieved. Thus, $\mathbf{w}^{(r)}$ is updated by

$$\mathbf{w}^{(r)} = \mathbf{w}^{\text{sub}}. \tag{42}$$

According to the analysis above, the MM Algorithm for solving P1.3 is summarized as Algorithm 2.

Algorithm 2 MM algorithm for solving the problem P1.3

1: **Initialize**: iteration index $\iota = 0$, iteration tolerance $\varepsilon > 0$, initial point $\mathbf{w}^{(0)}$;
2: **repeat**
3:    $\iota = \iota + 1$;
4:    Update $\mathbf{w}^{(\iota)}$ according to (41);
5: **until** $\|\mathbf{w}^{(\iota)} - \mathbf{w}^{(\iota-1)}\| < \varepsilon$
6: **Output**: $\mathbf{w}^{(\iota)}$.

Based on the analytical results above, Algorithm 3 is proposed to solve the problem P1. As a result, the optimized $\boldsymbol{\theta}$ and $\mathbf{w}$ under the given $\mathbf{p}$ are attained. Correspondingly, $\boldsymbol{\theta}^{(t)}$ and $\mathbf{w}^{(t)}$ are updated by

$$\boldsymbol{\theta}^{(t)} = \boldsymbol{\theta}^{(r)}, \mathbf{w}^{(t)} = \mathbf{w}^{(r)}. \tag{43}$$

Algorithm 3 BF design for solving the problem P1

1: **Initialize**: tolerance ϵ_1, ϵ_2, the iteration number $l = 0, r$, the maximum iteration $l_{\max}, r_{\max}$, the convergence flag $f = 0$ and the penalty parameters $\rho^{(0)}, c$;
2: **repeat**
3:    $l = l + 1$;
4:    Initialize the objective function $F^{(0)} = 0$, the iteration number $r = 0$, initial points $\{\boldsymbol{\theta}^{(0)}, \mathbf{w}^{(0)}, \mathbf{z}^{(0)}\}$;
5:    **repeat**
6:       $r = r + 1$;
7:       For fixed $\{\boldsymbol{\theta}^{(r-1)}, \mathbf{w}^{(r-1)}\}$, update $\mathbf{z}^{(r)}$;
8:       For fixed $\{\mathbf{z}^{(r)}, \mathbf{w}^{(r-1)}\}$, update $\boldsymbol{\theta}^{(r)}$ according to Algorithm 1 and (33);
9:       For fixed $\{\mathbf{z}^{(r)}, \boldsymbol{\theta}^{(r)}\}$, update $\mathbf{w}^{(r)}$ according to Algorithm 2;
10:      Calculate $F^{(r)} = \sum_{i=1}^{K}\log\left(1 + \frac{p_iz_i}{\sum_{j\neq i}^{K}p_jz_j+\sigma^2}\right) - \frac{1}{2}\rho^{(l-1)}\sum_{i=1}^{K}\left(\sqrt{z_i} - \left|\mathbf{w}^{\mathrm{H}}(\mathbf{g}_i + \tilde{\mathbf{H}}_i\boldsymbol{\theta})\right|\right)^2$;
11:    **until** $\left|F^{(r)} - F^{(r-1)}\right| < \epsilon_2$ or $r > r_{\max}$
12:    Calculate $\Xi^{(r)} = \sum_{i=1}^{K}\left(\sqrt{z_i} - \left|\mathbf{w}^{\mathrm{H}}(\mathbf{g}_i + \tilde{\mathbf{H}}_i\boldsymbol{\theta})\right|\right)^2$;
13:    **if** $\Xi^{(r)} < \epsilon_1$ **then**
      Set $f = 1$;
   else:
      Update $\rho^{(l)} = c\rho^{(l-1)}$;
   end if
14: **until** $f = 1$ or $l > l_{\max}$
15: **Output**: if $f = 1$, output $\{\boldsymbol{\theta}^{(r)}, \mathbf{w}^{(r)}\}$.

IV. PA AND JOINT OPTIMIZATION SCHEME DESIGN

In this section, we firstly give the power allocation for joint optimization scheme design under given BF vectors. Then, based on the obtained PBF, ABF and PA, the joint design scheme for EE maximization is developed, and corresponding joint optimization algorithm is presented. Finally, the complexity and convergence of the algorithms are analyzed.

A. Solving $\mathbf{p}$ given $\{\mathbf{w}, \boldsymbol{\theta}\}$

For given $\{\mathbf{w}, \boldsymbol{\theta}\}$, with (11) and (7), the PA problem for joint design scheme is formulated as

$$\text{P2}: \max_{\mathbf{p}} \ J_4 = \frac{\sum_{i=1}^{K} \log\left(1 + \frac{p_k|\mathbf{w}^{\text{H}}(\mathbf{g}_k+\tilde{\mathbf{H}}_k\boldsymbol{\theta})|^2}{\sum_{j=k+1}^{K} p_j|\mathbf{w}^{\text{H}}(\mathbf{g}_j+\tilde{\mathbf{H}}_j\boldsymbol{\theta})|^2+\sigma^2}\right)}{\sum_{i=1}^{K} \nu p_i + P_{\text{C}}}$$

$$\text{s.t.} \ C_3, C_5. \tag{44}$$

Since the problem P2 is non-convex, it is hard to be solved directly. For this reason, we exploit the SCA method to tackle it. Using the SCA method, the non-convex numerator of objective function J_4 in (44) can be transformed into a convex one by leveraging the following lower-bound of the logarithmic function [39], [40]. To be specific, we have:

$$R_i = \log\left(1 + \frac{p_i\xi_i}{\sum_{j=i+1}^{K} p_j\xi_j + \sigma^2}\right)$$
$$\geq \omega_i \log\left(\frac{p_i\xi_i}{\sum_{j=i+1}^{K} p_j\xi_j + \sigma^2}\right) + \Omega_i, \tag{45}$$

where $\xi_i = |\mathbf{w}^{\text{H}}(\mathbf{g}_i + \tilde{\mathbf{H}}_i\boldsymbol{\theta})|^2 (i \in \mathcal{K})$, which is known for given $\{\mathbf{w}, \boldsymbol{\theta}\}$. The equality holds when $\gamma_i = \frac{p_i\xi_i}{\sum_{j=i+1}^{K} p_j\xi_j+\sigma^2}$. Here,

$$\omega_i = \frac{\gamma_i}{1 + \gamma_i},$$
$$\Omega_i = \log(1 + \gamma_i) - \frac{\gamma_i}{1 + \gamma_i} \log(\gamma_i). \tag{46}$$

According to (45), R_i is tightly lower bounded by

$$\hat{R}_i = \omega_i \log\left(\frac{p_i\xi_i}{\sum_{j=i+1}^{K} p_j\xi_j + \sigma^2}\right) + \Omega_i. \tag{47}$$

With (47), the optimization problem is relaxed and can be converted to a convex optimization problem by introducing $\tau_i = \log(p_i)$. Based on this, substituting (47) into (44), problem P2 is changed into

$$\hat{\text{P2}}: \max_{\boldsymbol{\tau}} \ J_5 = \frac{\sum_{i=1}^{K} \omega_i \log\left(\frac{e^{\tau_i}\xi_i}{\sum_{j=i+1}^{K} e^{\tau_j}\xi_j+\sigma^2}\right) + \Omega_i}{\sum_{i=1}^{K} \nu e^{\tau_i} + P_{\text{C}}}$$
$$= \frac{\sum_{i=1}^{K} \omega_i\left(\tau_i + \log\xi_i - \log(\sum_{j\neq i}^{K} e^{\tau_j}\xi_j + \sigma^2)\right) + \Omega_i}{\sum_{i=1}^{K} \nu e^{\tau_i} + P_{\text{C}}}$$
$$\text{s.t.} \ \tau_i \leq \log(P_{\max,i}), \forall i \in \mathcal{K}. \tag{48}$$

where $\boldsymbol{\tau} = [\tau_1, ..., \tau_K]^T$. Because log-sum-exp is convex [39], the numerator of J_5 is a concave function. Moreover, the denominator is a convex function. Furthermore, the constraint

is linear. Therefore, the problem $\hat{\text{P2}}$ is strictly pseudo-convex and will have a global optimal solution. Besides, this problem is also fractional, so we can utilize the factional programming theory to obtain the optimal solution. Correspondingly, $\hat{\text{P2}}$ becomes the following equivalent subtraction problem as

$$\bar{\text{P2}}: \max_{\boldsymbol{\tau}} \ J_6 = \sum_{i=1}^{K} \omega_i\left(\tau_i + \log\xi_i - \log(\sum_{j=i+1}^{K} e^{\tau_j}\xi_j + \sigma^2)\right)$$
$$+ \Omega_i - \eta\left(\sum_{i=1}^{K} \nu e^{\tau_i} + P_{\text{C}}\right)$$
$$\text{s.t.} \ \tau_i \leq \log(P_{\max,i}), \forall i \in \mathcal{K}$$
$$e^{\tau_i}\xi_i \geq (2^{r_{0,k}} - 1)\sum_{j=i+1}^{K} e^{\tau_j}\xi_j + \sigma^2 \tag{49}$$

where η is a non-negative weighted parameter. The problems $\bar{\text{P2}}$ and $\hat{\text{P2}}$ are equivalent. Hence, we only need to optimize the equivalent problem $\bar{\text{P2}}$ to obtain the solution of $\hat{\text{P2}}$. Given the initial value of $\boldsymbol{\tau}$ and the parameter η, the problem $\bar{\text{P2}}$ is strictly convex and thus it has a global solution. Hence, we can use the Dinkelbach method [41] to obtain the optimal solution of $\boldsymbol{\tau}$. With (49), the first-order derivative of J_6 w.r.t τ_k can be calculated as

$$\frac{\partial J_6}{\partial \tau_k} = \omega_k - e^{\tau_k} \sum_{i=1}^{k-1} \frac{\omega_i\xi_k}{\sum_{j=i+1}^{K} e^{\tau_j}\xi_j + \sigma^2} - \eta\nu e^{\tau_k}. \tag{50}$$

With (50), the solution of $\frac{\partial J_6}{\partial \tau_k} = 0$ can be given by

$$\tau_k^o = \log\left(\omega_k/(\sum_{i=1}^{k-1} \frac{\omega_i\xi_k}{\sum_{j=i+1}^{K} e^{\tau_j}\xi_j + \sigma^2} + \eta\nu)\right), \tag{51}$$

where $\{\omega_i\}$ and $\{\tau_j\}$ at the right-hand side of (51) can take the values of their previous iterations. Considering the maximum power and minimal rate constraints, τ_k needs to be rewritten as

$$\tau_k = \min\{\max\{\tau_k^o, \log(P_{\min,k})\}, \log(P_{\max,k})\}, \tag{52}$$

where $P_{\min,k} = (2^{r_{0,k}} - 1)\xi_k^{-1}(\sum_{j=k+1}^{K} e^{\tau_j}\xi_j + \sigma^2)$ is from the C_4 constraint.

Next, using the obtained τ_k and BCD method to update other PA coefficients $\{\tau_j, j \neq k\}$ alternately until they converge. With the obtained $\{\tau_k\}$, we utilize the Dinkelbach method to update η as

$$\eta = \frac{\sum_{i=1}^{K} \omega_i \log\left(\frac{e^{\tau_i}\xi_i}{\sum_{j=i+1}^{K} e^{\tau_j}\xi_j+\sigma^2}\right) + \Omega_i}{\sum_{i=1}^{K} \nu e^{\tau_i} + P_{\text{C}}} \tag{53}$$

until it converges. Then, we use the obtained $\boldsymbol{\tau}$ to update $\mathbf{p}$ as $\{p_k = e^{\tau_k}\}$. After that, we employ the obtained $\mathbf{p}$ to update $\{\omega_i\}$ and $\{\Omega_i\}$ by (46) until they converge. Finally, the suboptimal PA, $\mathbf{p}^{\text{sub}}$ is attained. Based on the above analysis, an effective iterative algorithm based on SCA, Dinkelbach and BCD methods is proposed to obtain the PA coefficients. The algorithm is summarized as Algorithm 4. With Algorithm 4, the solution of the problem P2 are updated by $\mathbf{p}^{(t)} = \mathbf{p}^{\text{sub}}$.

Algorithm 4 PA algorithm for solving the problem P2

1: **Initialize**: tolerance $\varepsilon_{SCA}, \varepsilon_{FP}, \varepsilon > 0$, the iteration number $v = 0$, the maximum iteration number v_{max} and initial point $p_k^{(0)}, \eta^{(0)}, \omega_i^{(0)}, \Omega_i^{(0)}$;

2: **repeat**

3:     $v = v + 1$;

4:     Initialize the iteration number $v_1 = 0$ and initial point $p_k^{(v_1)} = p_k^{(v-1)}, \tau_k^{(v_1)} = \log p_k^{(v_1)}$;

5:     **repeat**

6:        $v_1 = v_1 + 1$;

7:        Initialize the iteration number $v_2 = 0$ and initial point $p_k^{(v_2)} = p_k^{(v_1-1)}, \tau_k^{(v_2)} = \log p_k^{(v_2)}$;

8:        **repeat**

9:           $v_2 = v_2 + 1$;

10:          Update $\boldsymbol{\tau}^{(v_2)}$ according to (51) and (52);

11:        **until** $||\boldsymbol{\tau}^{(v_2)} - \boldsymbol{\tau}^{(v_2-1)}|| < \varepsilon$

12:        Update $\tau_k^{(v_1)} = \tau_k^{(v_2)}$;

13:        Update $\eta^{(v_1)}$ by (53);

14:     **until** $|\eta^{(v_1)} - \eta^{(v_1-1)}| < \varepsilon_{FP}$

15:     $p_k^{(v_1)} = e^{\tau_k^{(v_1)}}$;

16:     Update $p_k^{(v)} = p_k^{(v_1)}$;

17:     Calculate $\omega_i^{(v)}, \Omega_i^{(v)}$ by (46);

18: **until** $\max_{i \in \mathcal{K}} \left\{ |\omega_i^{(v)} - \omega_i^{(v-1)}|, |\Omega_i^{(v)} - \Omega_i^{(v-1)}| \right\} < \varepsilon_{SCA}$

19: **Output**: $\mathbf{p}^{(v)}$.

B. Joint optimization algorithm

Based on the analytical results above, a joint resource allocation scheme for EE maximization is developed, and the corresponding algorithm is proposed to solve the optimization problem P0. As a result, the suboptimal PA, PBF and ABF are attained. The specific joint algorithm design is illustrated as Algorithm 5.

Algorithm 5 Joint optimization algorithm for solving the problem P0

1: **Initialize**: tolerance ϵ_{BCD}, the iteration number $t = 0$, the maximum iteration t_{max} and initial point $\{\mathbf{p}^{(0)}, \boldsymbol{\theta}^{(0)}, \mathbf{w}^{(0)}\}$;

2: **repeat**

3:     $t = t + 1$;

4:     For given $\mathbf{p}^{(t-1)}$, update $\{\boldsymbol{\theta}^{(t)}, \mathbf{w}^{(t)}\}$ according to Algorithm 3;

5:     For given $\{\boldsymbol{\theta}^{(t)}, \mathbf{w}^{(t)}\}$, update $\mathbf{p}^{(t)}$ according to Algorithm 4;

6:     Calculate the value of objective function $\Gamma^{(t)} = \eta_{EE}$ in problem P0;

7: **until** $|\Gamma^{(t)} - \Gamma^{(t-1)}| < \epsilon_{BCD}$ or $t > t_{max}$

8: **Output**: $\{\mathbf{p}^{(t)}, \boldsymbol{\theta}^{(t)}, \mathbf{w}^{(t)}\}$.

C. Complexity and convergence analysis

In this subsection, we give the complexity and convergence analysis. For the proposed optimization algorithm of joint design of PA, PBF and ABF, i.e., Algorithm 5, its complexity is mainly from the Algorithms 3 and 4. For the Algorithm 3, the complexity is mainly from Algorithms 1 and 2 as well as the iteration of CCCP method. Regarding the Algorithm 1, it mainly involves the iteration of MM method and EVD of matrix, and the corresponding complexity is approximated as $\mathcal{O}\left(M^3 + M^2 I_1\right)$, where I_1 is the iterative number of Algorithm 1. Similarly, the complexity of Algorithm 2 is approximated as $\mathcal{O}\left(N^3 + N^2 I_2\right)$, where I_2 is the iterative number of Algorithm 2. Thus, the complexity of Algorithm 3 is approximated as $\mathcal{O}\left((M^3 + M^2 I_1 + N^3 + N^2 I_2 + K I_3^{(1)}) I_3^{(2)} I_3^{(3)}\right)$, where $I_3^{(1)}$ is the iteration of CCCP method, $I_3^{(2)}$ and $I_3^{(3)}$ are the numbers of outer and outermost iterations of Algorithm 3, respectively. In Algorithm 4, the main calculation burden involves three-loop iterations of K devices, i.e., the innermost iteration of BCD method, inner iteration of Dinkelbach method and outer iteration of SCA method. Correspondingly, its complexity is approximated as $\mathcal{O}\left(K I_4^{(1)} I_4^{(2)} I_4^{(3)}\right)$, where $I_4^{(1)}$, $I_4^{(2)}$ and $I_4^{(3)}$ are the numbers of innermost, inner and outer iteration of Algorithm 4, respectively. Hence, based on the above analysis, the complexity of Algorithm 5 is approximated as $\mathcal{O}(((M^3 + M^2 I_1 + N^3 + N^2 I_2 + K I_3^{(1)}) I_3^{(2)} I_3^{(3)} + K I_4^{(1)} I_4^{(2)} I_4^{(3)}) I_5)$, where I_5 is the iterative number of the outermost BCD method.

In what follows, the convergence analysis of proposed joint optimization algorithm (Algorithm 5) is addressed. Due to the power limitation, the sum rate is also limited. Hence, the value of EE is upper-bounded. Moreover, for the t-th iteration, it can be concluded that

$$
\begin{aligned}
\Upsilon_1 : \quad & \Gamma\left(\mathbf{p}^{(t-1)}, \mathbf{w}^{(t)}, \boldsymbol{\theta}^{(t)}\right) \geq \Gamma\left(\mathbf{p}^{(t-1)}, \mathbf{w}^{(t-1)}, \boldsymbol{\theta}^{(t-1)}\right), \\
\Upsilon_2 : \quad & \Gamma\left(\mathbf{p}^{(t)}, \mathbf{w}^{(t)}, \boldsymbol{\theta}^{(t)}\right) \geq \Gamma\left(\mathbf{p}^{(t-1)}, \mathbf{w}^{(t)}, \boldsymbol{\theta}^{(t)}\right)
\end{aligned}
\tag{54}
$$

where Υ_1 holds for the convergence of the Algorithm 2, and Υ_2 holds for the convergence of the SCA algorithm. For the Algorithm 2, its convergence analysis is shown as follows. For the given $\rho^{(l-1)}$, it can be concluded that

$$
\begin{aligned}
\tilde{\Upsilon}_1 : \quad & F\left(\mathbf{w}^{(r-1)}, \boldsymbol{\theta}^{(r-1)}, \mathbf{z}^{(r)}\right) \geq F\left(\mathbf{w}^{(r-1)}, \boldsymbol{\theta}^{(r-1)}, \mathbf{z}^{(r-1)}\right), \\
\tilde{\Upsilon}_2 : \quad & F\left(\mathbf{w}^{(r-1)}, \boldsymbol{\theta}^{(r)}, \mathbf{z}^{(r)},\right) \geq F\left(\mathbf{w}^{(r-1)}, \boldsymbol{\theta}^{(r-1)}, \mathbf{z}^{(r)}\right), \\
\tilde{\Upsilon}_3 : \quad & F\left(\mathbf{w}^{(r)}, \boldsymbol{\theta}^{(r)}, \mathbf{z}^{(r)},\right) \geq F\left(\mathbf{w}^{(r-1)}, \boldsymbol{\theta}^{(r)}, \mathbf{z}^{(r)}\right)
\end{aligned}
\tag{55}
$$

where $\tilde{\Upsilon}_1$ holds for the convergence of the CCCP method [37], $\tilde{\Upsilon}_2$ holds for the convergence of the MM algorithm [38], and $\tilde{\Upsilon}_3$ holds for the convergence of the MM algorithm.

V. BENCHMARK SCHEME BASED ON THE MULTIDIMENSIONAL SEARCH AND ABC ALGORITHM

In this section, to evaluate the performance of the proposed joint resource allocation scheme in section IV, we present a benchmark scheme based on the multidimensional search method and ABC algorithm, where the power allocation is obtained by the K-dimensional search method, and the ABF and PBF are achieved by means of the ABC algorithm in [43], [44].

In order to deal with the ABF vector $\mathbf{w}$ and PBF vector $\boldsymbol{\theta}$ well, the optimization problem P0 in (11) can be equivalently

transformed into

$$\bar{\text{P}}0 : \max_{\{\mathbf{p},\tilde{\mathbf{w}},\boldsymbol{\theta}\}} \eta_{\text{EE}} = \frac{\sum_{i=1}^{K} \log\left(1 + \frac{p_i|\tilde{\mathbf{w}}^{\text{H}}(\mathbf{g}_i+\tilde{\mathbf{H}}_i\boldsymbol{\theta})|^2}{\sum_{j=i+1}^{K} p_j|\tilde{\mathbf{w}}^{\text{H}}(\mathbf{g}_j+\tilde{\mathbf{H}}_j\boldsymbol{\theta})|^2+N\sigma^2}\right)}{\sum_{k=1}^{K} \nu p_k + P_{\text{C}}}$$

$$\text{s.t. } \tilde{C}_2, C_3, C_4, C_5,$$

$$\tilde{C}_1 : |[\tilde{\mathbf{w}}]_n| = 1, \forall n \in \mathcal{N},$$

(56)

where $\tilde{\mathbf{w}} = \sqrt{N}\mathbf{w}$. Thus, $\boldsymbol{\theta}$ and $\tilde{\mathbf{w}}$ have the same CM constraint. Taking the C_3 constraint into account, we can employ the K-dimensional search method to find the optimal power allocation $p_k \in [0, P_{\text{max},k}]$ for $k \in \mathcal{K}$ to maximize the EE, where the power of each user p_k is uniformly quantized over the range of 0 and $P_{max,k}$ with smaller step size. Correspondingly, the search complexity is increased exponentially as K increases, and thus the complexity becomes high.

Considering that the dimensions of $\boldsymbol{\theta}$ and $\tilde{\mathbf{w}}$ are M and N, respectively, their sum dimension is high because of large M and N. Hence, for each searched power allocation $\mathbf{p}$, we use the ABC algorithm to achieve near-optimal solutions of $\boldsymbol{\theta}$ and $\tilde{\mathbf{w}}$ with maximum EE, i.e., $\boldsymbol{\theta}(\mathbf{p})$ and $\tilde{\mathbf{w}}(\mathbf{p})$. This is based on that the ABC algorithm is more suitable for solving the optimization problem with high-dimension variables [43], [44]. Specifically, for each value of $\mathbf{p}$ in the set $\Phi = \{\mathbf{p}|\mathbf{p} \in [0, P_{\text{max},1}] \times .... \times [0, P_{\text{max},K}]\}$, we can compute $\boldsymbol{\theta}(\mathbf{p})$ and $\tilde{\mathbf{w}}(\mathbf{p})$ by using the ABC algorithm. Then with the obtained $\mathbf{p}, \boldsymbol{\theta}(\mathbf{p}), and \tilde{\mathbf{w}}(\mathbf{p})$, we can decide whether these results satisfy the constrain conditions. If the conditions are satisfied, then we calculate the EE of the system, η_{EE}. Otherwise, η_{EE} is set equal to zero. By comparing all values of η_{EE}, we can find the optimal K indexes corresponding to maximum η_{EE}. With these K indexes, the optimal $\mathbf{p}^o, \boldsymbol{\theta}(\mathbf{p}^o), \tilde{\mathbf{w}}(\mathbf{p}^o)$ are achieved, and the corresponding joint resource allocation scheme is presented. For easy presentation, this benchmark scheme is referred as 'joint-scheme2', and the presented joint scheme in section IV is referred as 'joint-scheme1'. The joint-scheme2 can obtain superior performance over the joint-scheme1 because of near-optimal solution, but it has much higher complexity than the latter since the complicated multidimensional search method and ABC algorithm are employed to find the solution, especially when K is larger.

VI. SIMULATION RESULTS

In this section, we evaluate the effectiveness of the proposed resource allocation scheme for RIS-mmWave system in terms of EE performance through computer simulation. For the simulation setup, the BS and RIS are located at (0m, 0m) and (90m, 5m), respectively, and all devices are uniformly distributed in the circular area with (100m, 0m) as the center and the radius of 5m [23]. Unless otherwise specified, other main parameters are listed in Table I. Besides, $\lambda_{\text{U}} = 0$ dBi and $\lambda_{\text{B}} = 9.82$ dBi, and the relative gain of the RIS is $\nu = \frac{\lambda_{\text{I}}}{\sqrt{\lambda_{\text{B}}\lambda_{\text{U}}}} = 10$ dB [42] [22]. The carrier frequency is 28 GHz, $L_B = L_{k,I} = L_{k,B} = 4(\forall k \in \mathcal{K})$. The gains β_l follows a complex Gaussian distribution, i.e., $\beta_l \sim \mathcal{CN}(0, 10^{-0.1\mu_l(d)})$ and so are $\alpha_{k,l}$ and $\beta_{k,l}$, where $\mu_l(d) = a + 10b\log_{10}(d) + \xi$ dB, d is the distance in meters

between the transmitter and the receiver, the values of a, b and ξ are set to as $a = 61.4, b = 2, \xi = 5.8$ dB for LOS path and $a = 72, b = 2.92, \xi = 8.7$ dB for NLOS path [45]. $P_{\text{RIS}} =20$dBm [32], [33]. Simulation results are illustrated in Figs. 2-9, respectively. In simulation, the computer we used is an Intel(R) Core(TM) i7-9750H CPU @ 2.60GHz.

TABLE I
SIMULATION PARAMETERS

Parameters	Default Values
Number of devices	$K = 3$
Number of antennas at the BS	$N = 16$
Number of refection elements at the RIS	$M = 20$
Maximum power consumption	$P_{\text{max},k} = P_{\text{max}}$
Power amplifier coefficient	$\nu = 1/0.38$
Minimum rate constraint	$r_{0,k} = 0.5$b/s/Hz
Power consumption of the baseband	$P_{\text{BB}} = 200$ mW
Power consumption of the RFC	$P_{\text{RF}} = 160$ mW
Power consumption of the PS	$P_{\text{PS}} = 20$ mW
Power consumption of the LNA	$P_{\text{LNA}} = 40$ mW
Noise power	$\sigma^2 = -104$ dBm

In Fig. 2, we plot the EE performance of the system with the proposed schemes for different numbers of phase shift levels, where L=2, 8, K=2, the joint-scheme1 and the benchmark scheme (i.e., joint-scheme2) are compared. The continuous phase shift (i.e., $L = +\infty$) is also used as the performance upper bound to evaluate the discrete phase shift. From Fig. 2, it is found that the EE performance with discrete phase shifts is worse than that with continuous phase shifts, as expected, but it is increased with the increase of L. Namely, the system with L=8 has higher EE than that with L=2. This is because the larger is the value of L, the better is the adjustment on the IRS phase shifts. Thus, the discrete phase shift of RIS can be optimized well. Moreover, the system with L=8 can obtain the EE performance close to that of that with continuous phase shifts (L=+∞). Besides, the proposed joint-scheme1 can achieve the performance close to that of the benchmark scheme for different values of L, but the former has lower complexity than the latter because the latter needs the exhaustive multidimensional search method to achieve the near-optimal solution, while the former does not need this search method. Specifically, the latter needs average run time of 72215.09s, while the former only needs average run time of 1.28s. Based on these results above, we employ L=8 in the following figures taking the performance and complexity into account.

Fig. 3 gives the EE performance of the system with the proposed first scheme based on different PBF designs, including the particle swarm optimization (PSO) [46] based PBF scheme, the designed PBF scheme, and the random phase based PBF scheme (where the phase shifts of reflection coefficients in RIS are generated randomly), which are referred as "PSO PBF", "Designed PBF", and "Rand-phase PBF", respectively. From Fig. 3, we observe that our designed PBF scheme can obtain almost the same EE as the benchmark scheme of "PSO PBF", but it has lower complexity than the latter due to poor computational efficiency of latter, which can be seen from the run time. Namely, the former needs average run time of 0.0183s, while the latter needs average
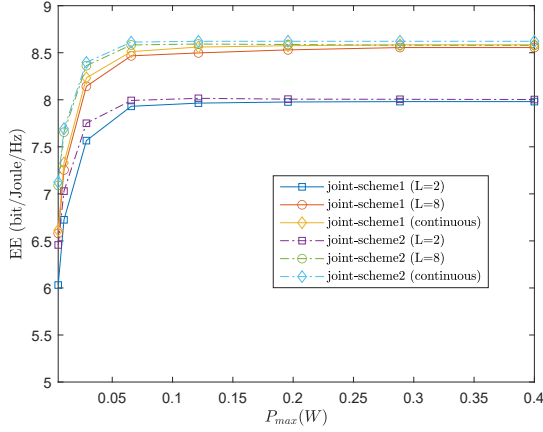
Fig. 2. EE of RIS-mmWave-NOMA with different numbers of phase shift levels.

Fig. 4. EE of RIS-mmWave-NOMA with different ABF schemes.

run time of 0.481s. Besides, "Designed PBF" and "PSO PBF" schemes both have much higher EE than the "Rand-phase PBF" scheme. This is because the PBF of "Rand-phase PBF" scheme is randomly generated and not optimized. The above results show effectiveness of the designed PBF scheme.
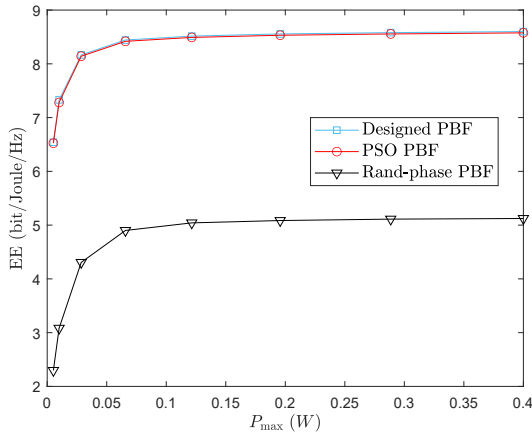

Fig. 3. EE of RIS-mmWave with different PBF schemes.

In Fig. 4, to illustrate the effectiveness of the designed ABF scheme, we give the EE comparison among the PSO based ABF scheme, the designed ABF scheme, codebook-based ABF scheme in [13], which are referred as "PSO ABF", "Designed ABF", and "Codebook ABF", respectively. It is shown in Fig. 4 that our designed ABF scheme and the benchmark scheme of "PSO ABF" both exhibit superior performance, and have much higher EE than the existing "Codebook ABF" scheme. This is because the BF vector in "Codebook ABF" scheme is selected from a finite set, and not always suitable for each channel realization. Besides, the designed scheme has almost the same EE as the benchmark scheme of "PSO ABF", but it has lower complexity than the latter. Specifically, the former needs average run time of 0.0045s, while the latter needs average run time of 0.387s.

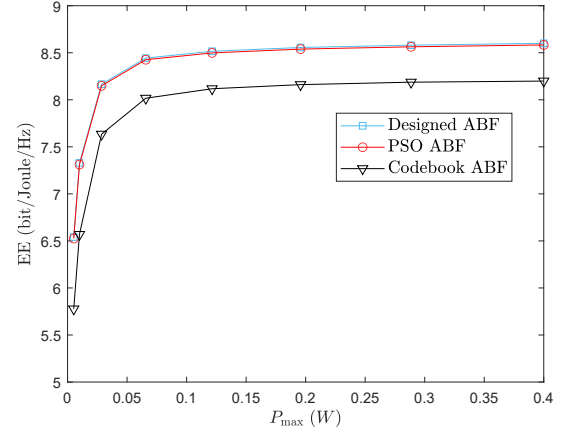In Fig. 5, we compare the EE of the system with different

numbers of RIS reflection elements, where the number of RIS reflection elements is set to $M = 0, 20, 40, 80$, and $M = 0$ means that RIS is not used. It is shown in Fig. 5 that the EE performance is improved as the number of reflection elements increases. Namely, the system with $M = 80$ obtains higher EE than that with $M = 40$, and the system with $M = 40$ obtains higher EE than that with $M = 20$. The reason is that the design of RIS reflection phase can provide the passive beamforming gain of RIS. Thus, with the increase of M, the higher passive beamforming gain can be attained. Besides, the system without RIS has the worst performance, and its EE is smallest. Hence, application of RIS does improve the EE performance effectively.
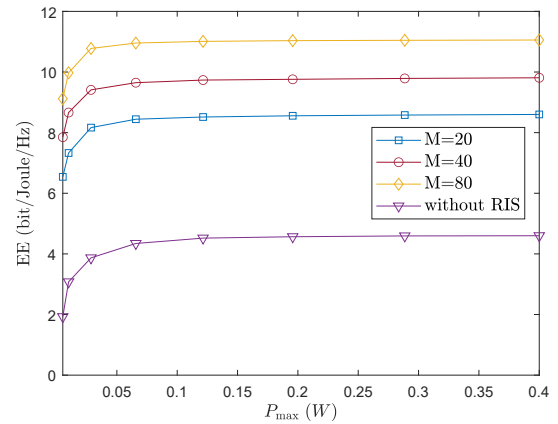

Fig. 5. EE of RIS-mmWave-NOMA with different numbers of RIS reflection elements.

Fig. 6 illustrates the EE of RIS-mmWave system with the proposed scheme under different numbers of antennas, where $N = 16, 32, 64$. As shown in Fig. 6, with the increase of antenna number N, the EE performance becomes worse. This is because the impact of total power consumption on the EE performance is more significant than the achievable sum rate when the antenna number is larger (which will result in the increase of total power consumption). The results above indicate that the proposed scheme is also valid for different
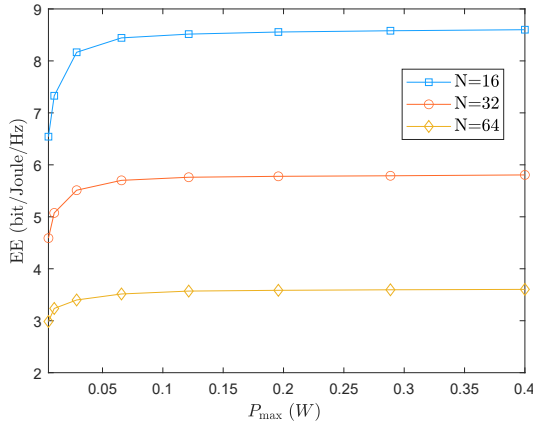
numbers of antennas.

Fig. 6.   EE of RIS-mmWave-NOMA with different numbers of antennas.

In Fig. 7, we plot the EE performance of the system with the proposed scheme for different numbers of devices, where the device number K=7, 9, 11. From Fig. 7, it is found that the EE is increased as the number of device increases, i.e., the EE with K=11 is higher than that with K=9, and the EE with K=9 is higher than that with K=7 since more devices are supported. The above results show that the proposed scheme is also effective for different numbers of device.
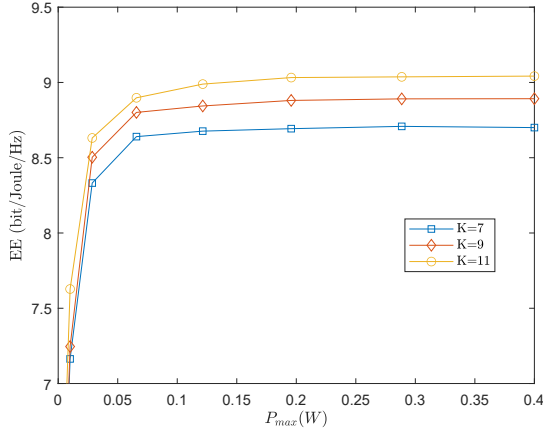

Fig. 7.   EE of RIS-mmWave-NOMA with different numbers of devices.

Fig. 8 shows the convergence behavior of the outermost iteration in the proposed joint optimization algorithm (Algorithm 5) for different values of P_{max}, where the EE versus the number of iterations is provided, and we set $P_{\max}$=0.02W, 0.4W. From Fig. 8, we can find that the EE is gradually increasing and finally saturated as the number of iteration increases for different values of $P_{\max}$. Thus, the outermost BCD convergence of Algorithm 5 is guaranteed. Moreover, after some iterations, two curves can converge to their respective optimal values, but these values are different. The value of EE with $P_{\max}$=0.4W is higher than that with $P_{\max}$=0.02W. Besides, their required iterations are different. Since $P_{\max}$=0.02W is low, the obtained PA is easily under

the maximum power constraint. Correspondingly, the EE curve with $P_{\max}$=0.02W converges faster than that with $P_{\max}$=0.4W. Specifically, the former needs about 3 iterations to converge, while the latter needs about 4 iterations to converge.
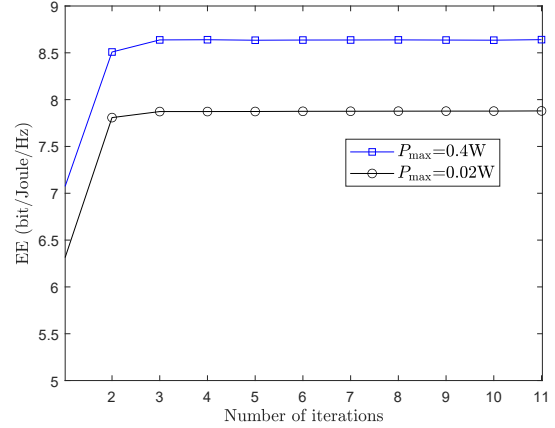

Fig. 8.   EE versus number of iterations

In Fig. 9, we evaluate the impact of imperfect CSI (I-CSI) on the EE performance of the RIS-aided mmWave-NOMA, where $r_{0,k}$=0. Following the statistical cascaded CSI estimation model in [29], [30], the cascaded channel matrix $\tilde{\mathbf{H}}_k$ and the channel vector $\mathbf{g}_k$ can be respectively modeled as $\tilde{\mathbf{H}}_k = \hat{\mathbf{H}}_k + \mathbf{E}_k$ and $\mathbf{g}_k = \hat{\mathbf{g}}_k + \boldsymbol{\epsilon}_k$, where $\hat{\mathbf{H}}_k$ and $\hat{\mathbf{g}}_k$ are the estimated channel matrix and vector, respectively, $\mathbf{E}_k$ and $\boldsymbol{\epsilon}_k$ are the corresponding CSI error matrix and vector, and they obey the circularly symmetric complex Gaussian distribution. Namely, $\text{vec}(\mathbf{E}_k) \sim CN(0, \sigma_k^2 \mathbf{I}_{MN})$, and $\boldsymbol{\epsilon}_k \sim CN(0, \varsigma_k^2 \mathbf{I}_N)$, where σ_k^2 and ς_k^2 are the variances of the corresponding CSI errors. According to [29], [30], $\sigma_k^2 = \mu_k^2 ||\text{vec}(\hat{\mathbf{H}}_k)||^2$ and $\varsigma_k^2 = \tilde{\mu}_k^2 ||\hat{\mathbf{g}}_k||^2$, where $\mu_k^2 \in [0, 1)$ and $\tilde{\mu}_k^2 \in [0, 1)$ are the normalized CSI errors that measure the CSI uncertainty level, and it is assumed that the normalized CSI errors of the users are the same for the convenience [29], [30], i.e., $\mu_k^2 = \mu^2$, and $\tilde{\mu}_k^2 = \tilde{\mu}^2$. In simulation, different errors $\mu^2 = \tilde{\mu}^2$=0.01^2, and $\mu^2 = \tilde{\mu}^2$=0.02^2 are considered, and for comparison, the EE performance under perfect CSI (P-CSI) is also provided. As illustrated in Fig. 9, the EE performance of the system becomes worse as the μ^2 and $\tilde{\mu}^2$ increase because of the degradation of CSI accuracy. Moreover, due to the CSI error, the system with I-CSI has lower EE than that with P-CSI, as expected.

VII. CONCLUSIONS

The joint resource allocation of PA, PBF and ABF is studied for maximizing the EE of uplink RIS-mmWave-NOMA network under the constraints of maximum power of devices and constant modulus of BF vectors. The joint optimization scheme with BCD method is developed to obtain the suboptimal PA, PBF and ABF. By means of MM method, CCCP and BCD method, suboptimal PBF and ABF are firstly designed given the PA, and an effective iterative algorithm is presented to obtain the suboptimal solutions. As a result, closed-form
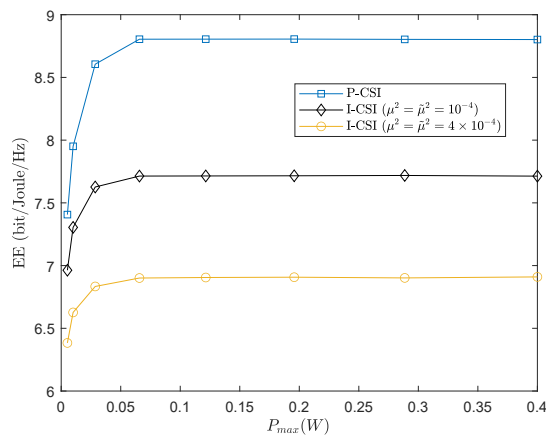
Fig. 9. EE of RIS-mmWave-NOMA with different normalized CSI errors

PBF and ABF are attained at each iteration. Then, given these two BFs, suboptimal PA is derived based on the SCA, Dinkelbach and BCD methods, and corresponding iterative algorithm is proposed for PA optimization, where closed-form PA is obtained at each iteration. By incorporating these two algorithms into the BCD method, a joint optimization algorithm for EE maximization is presented. With this algorithm, joint design of PA, PBF and ABF is implemented. Besides, the benchmark scheme is also presented based on the multidimensional search method and ABC algorithm for comparison. Simulation results illustrate that the proposed joint scheme is effective, and it can obtain superior EE performance over the random phase scheme and codebook scheme. Moreover, the proposed scheme has the EE performance close to the benchmark scheme but with lower complexity. Considering that the resource allocation scheme is based on perfect CSI, which is challenging to achieve, we will further study the optimization design of resource allocation for RIS-aided mmWave-NOMA network with imperfect CSI in our future work.

ACKNOWLEDGMENTS

REFERENCES

[1] X. Wang, L. Kong, F. Kong, F. Qiu, M. Xia, S. Arnon, G. Chen, "Millimeter wave communication: a comprehensive survey," *IEEE Commun. Surveys Tuts*, vol. 20, no. 3, pp. 1616-1653, 2018.

[2] A. N. Uwaechia and N. M. Mahyuddin, "A comprehensive survey on millimeter wave communications for fifth-generation wireless networks: Feasibility and challenges," *IEEE Access*, vol. 8, pp. 62367-62414, 2020.

[3] C. Pan, H. Ren, K. Wang, et al., "Reconfigurable intelligent surfaces for 6G systems: Principles, applications, and research directions," *IEEE Commun. Mag.*, vol. 59, no. 6, pp. 14-20, June 2021.

[4] Q. Wu and R. Zhang, "Towards smart and reconfigurable environment:Intelligent reflecting surface aided wireless network," *IEEE Commun. Mag.*, vol. 58, no. 1, pp. 106-112, Jan. 2020.

[5] X. Yu, V. Jamali, D. Xu, D. W. K. Ng, R. Schober, "Smart and reconfigurable wireless communications: From IRS modeling to algorithm design," *IEEE Wireless Commun.*, vol.28, no. 6, pp.118-125, Dec. 2021.

[6] G. Zhou, C. Pan, H. Ren, K. Wang, M. Elkashlan, M. Di Renzo, "Stochastic learning-based robust beamforming design for RIS-aided millimeter-wave systems in the presence of random blockages," *IEEE Trans. Veh. Technol.*, vol. 70, no. 1, pp. 1057-1061, Jan. 2021.

[7] L. Zhu, J. Zhang, Z. Xiao, et al., "Joint power control and beamforming for uplink non-orthogonal multiple access in 5g millimeter-wave communications," *IEEE Trans. Wireless Commun.*, vol. 17, no. 9, pp. 6177-6189, Sep. 2018.

[8] Z. Xiao, L. Zhu, Z. Gao, D. O. Wu, and X.-G. Xia, "User fairness non-orthogonal multiple access (NOMA) for millimeter-wave communications with analog beamforming," *IEEE Trans. Wireless Commun.*, vol. 18, no. 7, pp. 1536-1276, July 2019.

[9] S. M. R. Islam, N. Avazov, O. A. Dobre, and K. Kwak, "Power-domain non-orthogonal multiple access (NOMA) in 5G systems: Potentials and challenges," *IEEE Commun. Sur. Tuts.*, vol. 19, no. 2, pp. 721–742, 2017.

[10] C. Lin and G. Y. Li, "Energy-efficient design of indoor mmWave and sub-THz systems with antenna arrays," *IEEE Trans. Wireless Commun.*, vol. 15, no. 7, pp. 4660-4672, Jul. 2016.

[11] J. Guo, Q. Yu, W. Meng, and W. Xiang, "Energy-efficient hybrid precoder with adaptive overlapped subarrays for large-array mmwave systems," *IEEE Trans. Wireless Commun.*, vol. 19, no. 3, pp. 1484-1502, Mar. 2020.

[12] X. Yu, F. Xu, K. Yu and N. Li, "Joint energy-efficient power allocation and beamforming for uplink mmWave-NOMA system," *IEEE Trans. Veh. Technol.*, vol. 69, no. 10, pp. 12291-12295, Oct. 2020.

[13] W. Hao, M. Zeng, Z. Chu, and S. Yang, "Energy-efficient power allocation in millimeter wave massive MIMO with non-orthogonal multiple access," *IEEE Wireless Commun. Lett.*, vol. 6, no. 6, pp. 782-785, Dec. 2017.

[14] Z. Yang, M. Shikh-Bahaei and M. Chen et al., "Energy-efficient wireless communications with distributed reconfigurable intelligent surfaces," *IEEE Trans. Wireless Commun.*, vol. 21, no. 1, pp.665-679, Jan. 2022

[15] C. Huang, A. Zappone, G. C. Alexandropoulos, M. Debbah and C. Yuen, "Reconfigurable intelligent surfaces for energy efficiency in wireless communication," *IEEE Trans. Wireless Commun.*, vol. 18, no. 8, pp. 4157-4170, Aug. 2019.

[16] Q. N. Le, V. -D. Nguyen, O. A. Dobre and R. Zhao, "Energy efficiency maximization in RIS-aided cell-free network with limited backhaul," *IEEE Commun. Lett.*, vol. 25, no. 6, pp. 1974-1978, Jun. 2021.

[17] S. Hu, Z. Wei, Y. Cai, C. Liu, D. W. K. Ng, J. Yuan, "Robust and secure sum-rate maximization for multiuser MISO downlink systems with self-sustainable IRS," *IEEE Trans. Commun.*, vol.69, no.10, pp.7032-7049, Qct. 2021.

[18] Z. Zhang and L. Dai, "A joint precoding framework for wideband reconfigurable intelligent surface-aided cell-free network," *IEEE Trans. Signal Process.*, vol.69, no. 21, pp.4085-4101, 2021.

[19] C. Pan, H. Ren, K. Wang, W. Xu, M. Elkashlan, A. Nallanathan, and L. Hanzo, "Multicell MIMO communications relying on intelligent reflecting surfaces," *IEEE Trans. Wireless Commun.*, vol. 19, no. 8, pp.5218-5233, Aug. 2020.

[20] P. Wang, J. Fang, X. Yuan, Z. Chen and H. Li, "Intelligent reflecting surface-assisted millimeter wave communications: joint active and passive precoding design," *IEEE Trans. Veh. Technol.*, vol. 69, no. 12, pp. 14960-14973, Dec. 2020.

[21] C. Pradhan, A. Li, L. Song, B. Vucetic and Y. Li, "Hybrid precoding design for reconfigurable intelligent surface aided mmWave communication systems," *IEEE Wireless Commun. Lett.*, vol. 9, no. 7, pp. 1041-1045, Jul. 2020.

[22] Y. Cao, T. Lv, Z. Lin and W. Ni, "Delay-constrained joint power control, user detection and passive beamforming in intelligent reflecting surface-assisted uplink mmWave system," *IEEE Trans. Cogn. Commun. Netw.*, vol. 7, no. 2, pp. 482-495, Jun. 2021.

[23] R. Li, B. Guo, M. Tao, Y-F. Liu, W. Yu, "Joint design of hybrid beamforming and reflection coefficients in RIS-aided mmWave MIMO systems," *IEEE Trans. Commun.*, vol.70, no.4, pp.2404-2416, April 2022.

[24] J. Zuo, Y. Liu, E. Basar and O. A. Dobre, "Intelligent reflecting surface enhanced millimeter-wave NOMA systems," *IEEE Commun. Lett.*, vol. 24, no. 11, pp. 2632-2636, Nov. 2020.

[25] Z. Xiao, L. Zhu, J. Choi, et al., "Joint power allocation and beamforming for non-orthogonal multiple access (NOMA) in 5G millimeter wave communications," *IEEE Trans. Wireless Commun.*, vol. 17, no. 5, pp. 2961-2974, May. 2018.

[26] W. Zhang, J. Xu, W. Xu, D. W. K. Ng and H. Sun, "Cascaded channel estimation for IRS-assisted mmWave multi-antenna with quantized beamforming," *IEEE Commun.Lett.*, vol. 25, no. 2, pp. 593-597, Feb. 2021.

[27] Z. Chen, J. Tang, X. Y. Zhang, D. K. C. So, S. Jin, K.-K. Wong, "Hybrid evolutionary-based sparse channel estimation for IRS-assisted mmWave MIMO systems," *IEEE Trans. Wireless Commun.*, vol.21, no.3, pp.1586-1601, March 2022

[28] T. Lin, X. Yu, Y. Zhu, and R. Schober"Channel estimation for intelligent reflecting surface-assisted millimeter wave MIMO systems" *In Proc. 2020 IEEE Global Communications Conference (GLOBECOM 2020)*, pp.1-6, 2020.

[29] Y. Wang, X. Chen, Y. Cai, and L. Hanzo, "RIS-aided hybrid massive MIMO systems relying on adaptive-resolution ADCs: robust beamforming design and resource allocation," *IEEE Trans. Veh. Technol.*, vol.71, no.3, pp.3281-3286, March 2022.

[30] S. Hong, C. Pan, H. Ren, K.Wang, K. K. Chai, and A.Nallanathan, "Robust transmission design for intelligent reflecting surface-aided secure communication systems with imperfect cascaded CSI," *IEEE Trans. Wireless Commun.*, vol. 20, no. 4, pp. 2487-2501, Apr. 2021.

[31] Q. Wu and R. Zhang, "Beamforming optimization for wireless network aided by intelligent reflecting surface with discrete phase shifts," *IEEE Trans. Commun.*, vol. 68, no. 3, pp. 1838-1851, Mar. 2020.

[32] Q. Wang, F. Zhou, R. Q. Hu, and Y. Qian, "Energy efficient robust beamforming and cooperative jamming design for IRS-assisted MISO networks," *IEEE Trans. Wireless Commun.*, vol. 20, no. 4, pp. 2592-2607, Apr. 2021.

[33] X. Wu, J. Ma, Z. Xing, C. Gu, X. Xue and X. Zeng, "Secure and energy efficient transmission for IRS-assisted cognitive radio networks," *IEEE Trans. Cogn. Commun. Netw.*, vol. 8, no. 1, pp.170-185, Mar. 2022.

[34] S. J. Wright, "Coordinate descent algorithms," *Mathematical Programming*. vol.151, no.1, pp. 3-34. June 2015.

[35] A. Beck and L. Tetruashvili, "On the convergence of block coordinate descent type methods," *SIAM J. Optim.*, vol. 23, no. 4, pp. 2037-2060, 2013.

[36] C. Zhao, Y. Cai, A. Liu, M. Zhao and L. Hanzo, "Mobile edge computing meets mmWave communications: joint beamforming and resource allocation for system delay minimization," *IEEE Trans. Wireless Commun.*, vol. 19, no. 4, pp. 2382-2396, Apr. 2020.

[37] B. K. Sriperumbudur and G. R. Lanckriet, "On the convergence of the concave-convex procedure," in *Proc. Adv. Neural Inf. Process. Syst.*, 2009, pp.1759–1767.

[38] Y. Sun, P. Babu, and D. P. Palomar, "Majorization-minimization algorithms in signal processing, communications, and machine learning" *IEEE Trans. Signal Process.*, vol. 65, no. 3, pp. 794-816, Feb. 2017.

[39] S. Boyd and L. Vandenberghe, "Convex optimization," *Cambridge U.K.: Cambridge Univ. Press*, 2004.

[40] G. Dong, H. Zhang, S. Jin and D. Yuan, "Energy-efficiency-oriented joint user association and power allocation in distributed massive MIMO systems," *IEEE Trans. Veh. Technol.*, vol. 68, no. 6, pp. 5794-5808, Jun. 2019.

[41] W. Dinkelbach, "On nonlinear fraction programming," *Management Science*, vol 13, no. 7, pp. 492-298, 1967.

[42] H. Guo, Y.-C. Liang, J. Chen, and E. G. Larsson, "Weighted sumrate optimization for intelligent reflecting surface enhanced wireless networks," 2019. [Online]. Available: arXiv:1905.07920.

[43] Z.Xiao, H. Dong, L. Bai, et al., "Unmanned aerial vehicle base station (UAV-BS) eeployment with millimeter-wave beamforming," *IEEE Internet Things J.*, vol.7, no.2, pp.1336-1349, Feb. 2020.

[44] D. Karaboga and B. Basturk, "On the performance of artificial bee colony (ABC) algorithm," *Appl. Soft Comput.*, vol. 8, no. 1, pp. 687-697, Jan. 2008

[45] M. R. Akdeniz, Y. Liu, M. K. Samimi, et al., "Millimeter wave channel modeling and cellular capacity evaluation," *IEEE J. Sel. Areas Commun.*, vol. 32, no. 6, pp. 1164-1179, Jun. 2014.

[46] R. Poli, J. Kennedy, and T. Blackwell, "Particle swarm optimization," *Swarm Intell.*, vol. 1, no. 1, pp. 33–57, 2007.